

MAY 30 1980
JUL 22 1980

REPORT NO. NADC-78291-60

NADC-78291-60



THE AERODYNAMICS OF A JET IN A CROSSFLOW

K. T. Yen
Aircraft and Crew Systems Technology Directorate
NAVAL AIR DEVELOPMENT CENTER
Warminster, Pennsylvania 18974

December 11, 1978

FINAL REPORT
AIRTASK NO. A3203200/001A/9R023-02-000

APPROVED FOR PUBLIC RELEASE; DISTRIBUTION UNLIMITED

Prepared for
NAVAL AIR SYSTEMS COMMAND
Department of the Navy
Washington, D. C. 20361

Property of U. S. Air Force
AEDC LIBRARY
F40600-77-C-0003

C-1
PROPERTY OF U.S. AIR FORCE
AEDC TECHNICAL LIBRARY
ARNOLD AFB, TN 37389

79 11 - 07 - 001

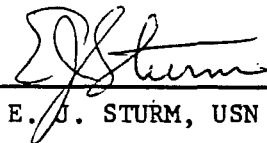
NOTICES

REPORT NUMBERING SYSTEM - The numbering of technical project reports issued by the Naval Air Development Center is arranged for specific identification purposes. Each number consists of the Center acronym, the calendar year in which the number was assigned, the sequence number of the report within the specific calendar year, and the official 2-digit correspondence code of the Command Office or the Functional Directorate responsible for the report. For example: Report No. NADC-78015-20 indicates the fifteenth Center report for the year 1978, and prepared by the Systems Directorate. The numerical codes are as follows:

CODE	OFFICE OR DIRECTORATE
00	Commander, Naval Air Development Center
01	Technical Director, Naval Air Development Center
02	Comptroller
10	Directorate Command Projects
20	Systems Directorate
30	Sensors & Avionics Technology Directorate
40	Communication & Navigation Technology Directorate
50	Software Computer Directorate
60	Aircraft & Crew Systems Technology Directorate
70	Planning Assessment Resources
80	Engineering Support Group

PRODUCT ENDORSEMENT - The discussion or instructions concerning commercial products herein do not constitute an endorsement by the Government nor do they convey or imply the license or right to use such products.

APPROVED BY:


E. J. STURM, USN

DATE:

9/19/79

REPORT DOCUMENTATION PAGE		READ INSTRUCTIONS BEFORE COMPLETING FORM
1. REPORT NUMBER NADC-78291-60	2. GOVT ACCESSION NO.	3. RECIPIENT'S CATALOG NUMBER
4. TITLE (and Subtitle) THE AERODYNAMICS OF A JET IN A CROSSFLOW		5. TYPE OF REPORT & PERIOD COVERED Final Report
		6. PERFORMING ORG. REPORT NUMBER
7. AUTHOR(s) K. T. Yen		8. CONTRACT OR GRANT NUMBER(s)
9. PERFORMING ORGANIZATION NAME AND ADDRESS Aircraft & Crew Systems Technology Directorate NAVAL AIR DEVELOPMENT CENTER (Code 60) Warminster, PA 18974		10. PROGRAM ELEMENT, PROJECT, TASK AREA & WORK UNIT NUMBERS AIRTASK NO. A3203200/ 001A/9R023-02-000
11. CONTROLLING OFFICE NAME AND ADDRESS Naval Air Systems Command Department of the Navy Washington, DC 20361		12. REPORT DATE December 11, 1978
		13. NUMBER OF PAGES 58
14. MONITORING AGENCY NAME & ADDRESS (if different from Controlling Office)		15. SECURITY CLASS. (of this report) UNCLASSIFIED
		15a. DECLASSIFICATION/DOWNGRADING SCHEDULE
16. DISTRIBUTION STATEMENT (of this Report) Approved for Public Release; Distribution Unlimited		
17. DISTRIBUTION STATEMENT (of the abstract entered in Block 20, if different from Report)		
18. SUPPLEMENTARY NOTES		
19. KEY WORDS (Continue on reverse side if necessary and identify by block number) V/STOL Aerodynamics Transition Aerodynamic Interference Jet		
20. ABSTRACT (Continue on reverse side if necessary and identify by block number) The aerodynamics of a jet in a crossflow considered as the key problem in transition aerodynamics for VSTOL aircraft has been reviewed. Experimental results on the flow structure of the jet, the contrarotating vortices, the jet entrainment phenomenon, and the surface pressure distributions have been analyzed. The influences on these characteristics by the jet parameters such as the velocity ratio, injection angle and jet orifice shape have been considered based on available measurements. In the theoretical area, particular		

UNCLASSIFIED

SECURITY CLASSIFICATION OF THIS PAGE (When Data Entered)

attention has been directed to the methods of prediction and analysis, and the fundamental physical bases of these methods. Current developments in transition aerodynamics, and some recent work on the formation of contrarotating vortices and the wake flow are described.

S/N 0102-LF-014-6601

UNCLASSIFIED

SECURITY CLASSIFICATION OF THIS PAGE (When Data Entered)

SUMMARY

The aerodynamics of a jet in a crossflow considered as the key problem in transition aerodynamics for VSTOL aircraft has been reviewed. Experimental results on the flow structure of the jet, the contrarotating vortices, the jet entrainment phenomenon, and the surface pressure distributions have been analyzed. The influences on these characteristics by the jet parameters such as the velocity ratio, injection angle and jet orifice shape have been considered based on available measurements. In the theoretical area, particular attention has been directed to the methods of prediction and analysis, and the fundamental physical bases of these methods. Current developments in transition aerodynamics, and some recent work on the formation of contrarotating vortices and the wake flow are described.

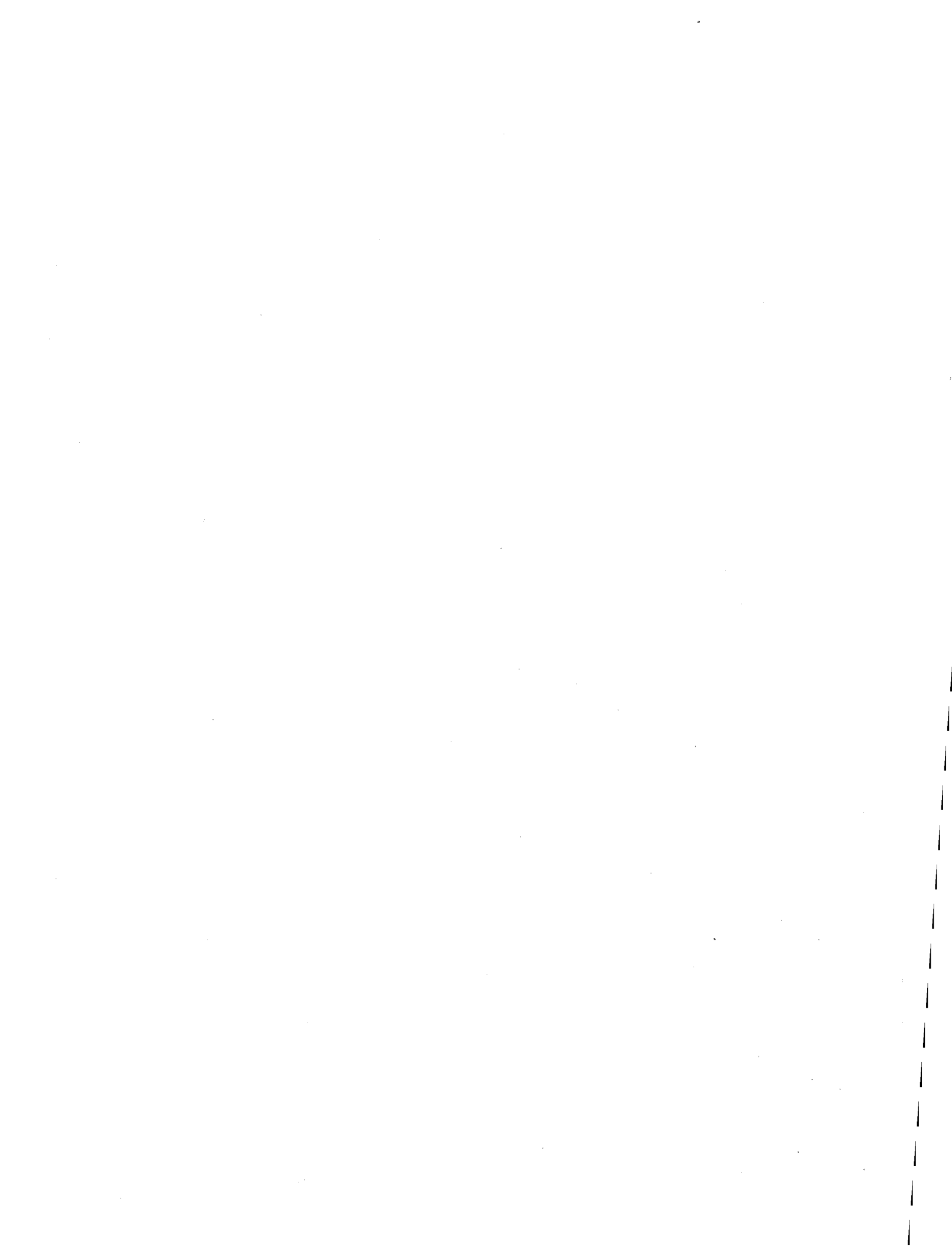


TABLE OF CONTENTS

	Page
SUMMARY	i
LIST OF FIGURES	2
LIST OF SYMBOLS	3
INTRODUCTION	6
GENERAL AERODYNAMIC CHARACTERISTICS	6
The Aerodynamic Structure of a Turbulent Jet in a Crossflow	8
The Surface Pressure Distributions	12
METHODS OF PREDICTION AND ANALYSIS	14
The 1969 NASA Symposium	15
The 1975 Navy Workshop	16
Wooler's Method	17
Snel's Method	19
Fearn and Weston's Method	19
CURRENT DEVELOPMENTS IN THE AERODYNAMICS OF A JET IN A CROSSFLOW AND TRANSITION AERODYNAMICS	20
Formation of Contrarotating Vortices	21
The Wake of a Jet in a Crossflow	25
Entrainment by Contrarotating Vortices	26
CONCLUDING REMARKS	27
REFERENCES	28

LIST OF FIGURES

Figure	Title	Page
1	A Jet in a Crossflow	31
2	Jet Path and Centerline for Various Velocity Ratios	32
3	Total Pressure Contours at Station I, $R = 6$	33
4	Total Pressure Contours at Station IV, $R = 6$	33
5	Contours of Constant Velocity, $R = 8$, $\xi/D = 12.5$ and 23	34
6	Rotational Velocity Field in Vortex Region, $R = 8$ and $\xi/D = 12.5$	35
7	Jet Centerline and Vortex Trajectory	36
8	Vortex Strength Distributions (Fearn and Weston, reference 13)	37
9	Distribution of Velocity Along the Jet Centerline	38
10	Lateral Spread of Heated Jet	39
11	Mass Flux Distributions	40
12	Entrainment Velocity Distributions	41
13	Variation of Entrainment With the Velocity Ratio U_∞/U_{j0} (reference 27)	42
14	Jet Orifice Configurations (reference 19)	42
15	Jet Paths With Injection Angle $\omega = 90^\circ$	43
16	Estimated Jet Paths Based on Taylor's Measurements (reference 21) for Various Injection Angles	44
17	Static Pressure Distribution	45
18	Contours of Constant c_p , $R = 7.0$	46
19	Estimates of the Size of the Three Regions Versus the Velocity Ratio R	47
20	Locations of Minimum Pressure Point and Separation Point Versus the Velocity Ratio R	48
21	Oil Film Photograph for $w/l = 1.0$, $R = 12$ (reference 19)	49
22	Oil Film Pattern on the Plate From Which a Jet is Issued Into a Crossflow	49
23	Composite of c_p Contours (reference 19)	50
24	Comparison of Entrainment Coefficients	51
25	Pressure Distribution Around a Single Jet Issuing at an Angle $\omega = 90^\circ$, $R = 8$	52
26	Pressure Distribution Around a Single Jet Issuing at an Angle $\omega = 90^\circ$, $R = 8$	53
27	Pressure Distribution Around a Single Jet Issuing at an Angle $\omega = 90^\circ$, $R = 8$	54
28	A Sketch of the Flow Pattern	55
29	Location of the Wake Vortices	56
30	Flow Over a Body - Closed Streamlines	57
31	Flow With Open Streamlines	58

LIST OF SYMBOLS

A	Area ratio
A_j	Jet cross sectional area
C_D	Drag coefficient, equation (14)
c_p	Static pressure coefficient
c_{pt}	Total pressure coefficient
d	Jet width
D	Diameter of the circular jet orifice
E	Entrainment coefficient, equation (10)
E_1, E_2	Entrainment coefficients, equation (11)
E_c, E_p, E_a	Entrainment coefficients, equation (15)
h	Half lateral spacing of the vortex curve
h_0	Empirical constant, equation (6)
k	Curvature of the jet centerline
ℓ	Length of the jet orifice
ℓ_e	Perimeter of the turbulent flow region
m	Mass flux of the jet
M_j	Mach number of the jet at exit
M_∞	Free-stream Mach number
p	Static pressure
p_∞	Free-stream static pressure
P	Static pressure at the jet boundary
q_∞	Free-stream dynamic pressure
r, ϕ , z	Cylindrical coordinates
$r_{1/2}$	Half-value radius, equation (8)
R	Velocity ratio (U_{j0}/U_∞)

Re	Reynolds number
s	Length measured along the vortex curve
S	Separation point
$S_{1/2}$	Area occupied by the contour of half-value radius $r_{1/2}$
T	Temperature
T_0	Jet exit temperature
T_∞	Free-stream temperature
u, v, w	Velocity components in x, y, z directions, respectively
u*	Dimensionless velocity, equation (2)
U	Jet velocity
U_e	Entrainment velocity, equation (9)
U_j	Velocity at the jet centerline
U_{j0}	Velocity at the jet exit
U_{max}	Maximum value of U
U_∞	Free-stream velocity
V	Swirling velocity at the jet boundary
w	Width of the jet orifice
W	Axial velocity at the jet boundary
x, y, z	Cartesian coordinates, figure 1
α	Angle in a jet cross section measured from the forward stagnation point
α_p	Angular location of the surface minimum pressure
α_s	Angular location of the separation point
β	An empirical constant, equation (6)
γ	Dimensionless vortex strength ($\Gamma/2U_\infty D$)
Γ	Vortex strength
δ	Jet boundary

θ	Angle between the jet centerline and x-axis
λ	Axial jet velocity parameter, equation (32)
μ	Coefficient of viscosity
ξ, η, ζ	Coordinates attached to the jet centerline, figure 1
ρ	Density
σ	Dimensionless temperature of the jet
τ	Shear stress
τ^*	Dimensionless shear stress
ϕ	Azimuthal coordinate
χ	Dimensionless boundary layer thickness (r/δ)
ω	Injection angle of the jet

INTRODUCTION

With the development of VSTOL aircraft, increasing attention has been directed to aerodynamic interference effects produced by propulsive devices especially during hover and transition flight. The origin, nature, and magnitude of these effects have been appraised by Williams and Wood in 1966 (reference 1). Some of the major aerodynamic problems and design requirements facing the aircraft designer have been reviewed by Margason in 1970 (reference 2). The methods of solution for these problems available at that time have also been described by Margason. Although considerable progress has been achieved in recent years in the understanding and solution of the aerodynamic interference problem, primarily through wind tunnel measurements and experiments, reliable methods of aerodynamic analysis, prediction or design are not yet available. A comprehensive review of current prediction methods for jet VSTOL propulsion aerodynamics has been presented by Platzer and Margason in reference 3.

The present work, as a part of a major task being conducted at the Naval Air Development Center (NADC) in an overall assessment of VSTOL aerodynamics, is directed to the transition aerodynamics. In the regime of transition flight, in which a VSTOL aircraft has attained some forward speed, a substantial portion of the lift is provided by the propulsion devices; i.e., the jet or fan efflux. The interference problems, in particular the lift loss and adverse pitching moment, for several typical VSTOL configurations have been studied in many experimental investigations carried out at NASA/Langley (references 2, 4, 5 and 6, e.g.). A key element of the aerodynamic interference is the interaction of a turbulent jet with the free-stream crossflow. Development of a satisfactory transition aerodynamic theory has been hampered by the complexities of the interaction involving the jet deflection, flow entrainment by the jet, formation of the contrarotating vortices, and the wake flow.

In the present study, all available theoretical and experimental work on the aerodynamics of a jet in a subsonic crossflow has been reviewed in some depth. The purpose is to delineate and define the essential features of the aerodynamic interaction phenomenon, the problem areas, and the additional work, both experimental and theoretical, needed for the solution. Particular attention has been directed to the analytical bases of current prediction methods in an attempt to assess their capabilities and deficiencies. Current efforts and progress towards the development of new and improved prediction methods are described.

GENERAL AERODYNAMIC CHARACTERISTICS

The aerodynamic characteristics of the turbulent jet in a crossflow have been studied in numerous experimental investigations in wind tunnels. Results up to 1969 have been reviewed by Skifstad (reference 7). Earlier experiments were directed mainly to the determination of the path of the jet (references 8 and 9). More recently, detailed measurements of the flow structure of a jet issuing normally from a large flat plate into a crossflow have been carried out by Jordinson (reference 10), Keffer and Baines (reference 11), Kamotani and Greber (reference 12), Fearn and Weston (references 13 and 14), and Antani (reference 15). Surface pressure distributions at the plate have been

measured by Bradbury and Wood (reference 16), Vogler (reference 17), Wu, McMahon, Mosher and Wright (reference 18), Mosher (reference 19), Fearn and Weston (reference 20), and Taylor (reference 21).

Evidently, the problem of a jet issuing from a flat plate into a cross-flow is the simplest one which still retains the essential features of the interaction problem (figure 1). Only a limited number of studies are available for a jet issuing from a wing (references 4, 22 and 23) or a body of revolution (reference 24).

The interaction between a turbulent jet and a subsonic crossflow in the presence of a large plate is characterized by, in addition to the bending and spreading of the jet and the formation of contrarotating vortices, the development of a wake region near the surface with a very complex flow structure.

Although the measurements cited above have contributed significantly to the present understanding of the jet in a crossflow problem, a serious gap still exists for the wake flow region near the jet exit. The main reason is that although the pressure measurements have been made close to the jet exit, mostly the measurements on the flow structure of the jet were conducted too far downstream from the exit. Only in a recent thesis by Antani at the Georgia Institute of Technology (reference 15), are some measurements in the wake region reported. Noteworthy, however, is the oil-film study of Mosher (reference 19), which has revealed many significant features of the wake flow near the surface, and contributed to the development of a wake model to be discussed later in this report.

In the following, experimental results in two areas; i.e., jet flow structure and surface pressure distributions, will be reviewed first. Significant features of the jet interaction problem which have been deduced from these results (as well as from other studies) will then be discussed. All the experimental results to be reviewed are for the case in which the jet issues from a large flat plate. The significant parameters and quantities governing the interaction phenomenon are:

$$\text{Velocity Ratio } R = \frac{\text{Typical Jet Velocity}}{\text{Free-Stream Velocity}}$$

$$\text{Area Ratio } A = \frac{\text{Area of the Plate}}{\text{Jet Orifice Area}}$$

Mach Numbers M_j and M_∞ of the Jet and Free Stream, respectively

Shape of the Jet Orifice

Injection Angle of the Jet ω

In the present study, the area ratio A is regarded as very large (as is generally the case for the experiments under review), and the compressibility effects are not taken into consideration. Thus, only the velocity ratio, the injection angle and the jet orifice shape are the significant parameters. The velocity ratio will be taken as $R = U_{j0}/U_\infty$, where U_{j0} is a typical jet velocity at the exit, and U_∞ is the free stream velocity.

THE AERODYNAMIC STRUCTURE OF A TURBULENT JET IN A CROSSFLOW

Several different approaches have been used for probing the structure of the jet. The earlier approach by Jordinson (reference 10) was to measure the total pressure distributions, and the results were given in the form of contours of total pressure coefficient c_{pt} defined by

$$c_{pt} = \frac{\text{Measured total pressure} - \text{Free-stream total pressure}}{\text{Jet total pressure} - \text{Free-stream total pressure}} \quad (1)$$

Results for the locations of the jet path (defined as the locus of maximum c_{pt}) and jet boundaries, and c_{pt} contours at various stations along the jet path for R values of 4, 6, and 8 were given by Jordinson for a jet issuing from a circular orifice. Figure 2 shows Jordinson's results for the jet path. For comparison, Fearn and Weston's results for the jet centerline defined as the locus of the maximum velocity in the plane of symmetry (reference 14) are also plotted in figure 2.

Contrarotating Vortices

Two of Jordinson's total pressure plots for R = 6 at Stations I and IV (figure 2) are shown in figures 3 and 4. Station I is fairly close to the jet orifice and situated at nearly two jet diameters above, while Station IV is at a vertical plane about five diameters downstream. Typically in the jet region, the total pressure is positive, while downstream of the jet there is a region of negative c_{pt} , which can be identified as the wake. The presence of two wake vortices is noted in figure 3, but the contrarotating jet vortices are not easy to discern. At downstream stations (e.g., figure 4), the wake vortices are not observed (see also figure 29).

The reason that the total pressure contours are not necessarily the best means to show the contrarotating vortices in the jet can be seen by examining the expression for c_{pt} , equation (1). The numerator is the sum of two terms: $p - p_\infty$ and $\rho(U^2 - U_\infty^2)/2$, where p and U are the measured static pressure and velocity, respectively, and the subscript ∞ denotes the quantity at free stream. Within the jet, the pressure difference is generally negative, especially near the vortex center, while the velocity square difference term is positive. Thus, generally c_{pt} does not have an extremum at the vortex center, and the contrarotating vortices may not be visible in a total pressure plot. In the wake, however, both the two difference terms are negative, leading to a more conspicuous vortex picture (provided the vortices are sufficiently strong). In more recent experiments on the jet vortex structure by Kamotani and Greber (reference 12), and Fearn and Weston (references 13 and 14), velocity measurements were used and found to be a more direct and convenient method to show the vortex structure.

In the experiments carried out by Kamotani and Greber (references 12 and 25), special care was taken to insure flat initial velocities at the jet orifice with low turbulence intensity. Near the exit, the jet exhibits a "potential core" in which the velocity is nearly uniform. With the development of the contrarotating vortices, the maximum velocity shifts from the

midplane to the vortex centers. Kamotani and Greber measured, for the velocity ratio R ranging approximately from 4 to 7.72, the time average velocity U , and obtained graphs for the non-dimensionalized velocity u^*

$$u^* = \frac{U - U_\infty}{U_{\max} - U_\infty} \quad (2)$$

Figure 5 shows their graph of constant velocity contours in a normal plane at a distance of $12.5D$ from the jet exit along the jet centerline for $R = 8$. The coordinates η and ζ are measured from the jet centerline (figure 1). In the jet region, the value of u^* lies between 0 and 1, and u^* is negative in the wake region. Also marked by a cross is the vortex center estimated from the rotational velocity field shown in figure 6 (reproduced from figure 22 of reference 25). Clearly, graphs of constant velocity contours serve quite well to reveal the vortex structure. Kamotani and Greber have also measured the turbulence intensity of the jet flow, and found the intensity to be highest near the vortex centers and the turbulence level as a whole higher with increasing velocity ratio. In a recent experimental study, Fearn and Weston (reference 14) adopted a very useful method of representation by plotting in the same graph, both contours of constant velocity component perpendicular to the cross section and a vector plot of the projections of measured velocities onto the cross section.

Additional information for the vortices have been provided by Fearn and Weston (reference 14) and Antani (reference 15). Fearn and Weston have developed a diffuse vortex model and shown it to be adequate in representing the measured induced velocity field at various cross sections along the jet centerline for several velocity ratios ($3 < R < 10$). They gave the following empirical equations for the trajectories and strengths of the vortice, which were found to fit experimental results quite well:

Vortex Curve

$$Z/D = 0.347R^{1.127}(x/D)^{.429} \quad (3)$$

Vortex Strength $\Gamma = 2U_\infty D \gamma$

$$\gamma = 0.72R \operatorname{erf}(\beta h_0) \quad (4)$$

Lateral Spacing $2h$

$$h = h_0 / \operatorname{erf}(\beta h_0) \quad (5)$$

$$\text{where } h_0 = 2.04D \left(1 - e^{-s/DR}\right) \quad (6)$$

$$\beta = 2.11/(sD)^{\frac{1}{2}} \quad (7)$$

and s is measured along the vortex curve.

The vortex curve together with the jet centerline is shown in figure 7. The contrarotating vortices can be detected easily 45 jet diameters downstream

of the jet orifice, but the jet centerline may be detectable to about 15 jet diameters according to Fearn and Weston. Figure 8 shows the variation of the vortex strength along the vortex curve for two values of R . It is apparent that the vortex strength will build up starting from the jet exit, reach a maximum value at several jet diameters downstream, and then begin to decay. Unfortunately, not enough experimental results near the jet exit region are available at the present time to give much information about the origin and formation of the contrarotating vortices. The diffuse model is undoubtedly a valid pseudo two-dimensional vortex model appropriate for the induced velocity field. Recently, Antani found the vorticity distribution in the jet is indeed very diffuse, and there was no evidence of vorticity concentration at the vortex centers (reference 15).

Entrainment

Turbulent mixing is an important aspect of the interaction phenomenon between a jet and a crossflow producing the entrainment of the free stream into the jet, and the spread and decay as well as bending of the jet.

Kamotani and Greber's results (reference 12) for the axial velocity along the jet centerline is shown in figure 9. The potential core for the free jet is about five jet diameters in length, while those of the jet in a crossflow are considerably shorter. The decay of the jet centerline velocity in a crossflow depends on the velocity ratio in a sensitive manner. Kamotani and Greber studied the temperature spread in a heated jet. As a measure of temperature spread, the half-value radius $r_{1/2}$ is defined as

$$r_{1/2} = (S_{1/2}/\pi)^{1/2} \quad (8)$$

where $S_{1/2}$ is the area occupied by the contour $\sigma = 0.5$, where $\sigma = (T - T_\infty)/(T_{\max} - T_\infty)$, and T_∞ is the free-stream temperature. Figure 10 shows the distribution of $r_{1/2}$ for two values of R and the jet exit temperature 320°F above the free-stream temperature. Note that initially the temperature in a jet in a crossflow spreads faster than that in a free jet, but slower farther downstream. Thus, in terms of the entrainment the jet in a crossflow problem is a more complex one than that of a free jet.

The rate of increase of the mass flux in the turbulent jet is given by

$$dm/d\xi = \rho l_e U_e \quad (9)$$

where l_e is the perimeter of the turbulent region at ξ , and U_e is the entrainment velocity representing the speed at which the turbulent front increases downstream. U_e is of primary interest, but is determined from the measured values of ρ , l_e and m . Figure 11 shows Kamotani and Greber's results for the mass flux distributions, and figure 12 the deduced entrainment velocity.

It is convenient to introduce entrainment coefficients, since U_e is dependent on the velocity field. For a free jet, an entrainment coefficient

is defined by

$$U_e = E(U_{\max} - U_{\infty}) \quad (10)$$

where U_{\max} is the maximum jet velocity at the station ξ . E is expected to depend on the distance measured from the jet exit, and has to be determined experimentally (see reference 26, e.g.). For a jet in a crossflow, Kamotani and Greber introduced two entrainment coefficients as follows:

$$U_e = E_1(U_{\max} - U_{\infty}\cos\theta) + E_2 U_{\infty}\sin\theta \quad (11)$$

where θ is the angle between the jet centerline and the x-axis. E_1 is the parallel-jet entrainment coefficient analogous to E in equation (10). $U_{\infty}\sin\theta$ and E_2 are the cross-jet velocity and entrainment coefficient, respectively. A similar expression for U_e has been used by Wooler, Burghart and Gallagher (reference 22).

Kamotani and Greber gave the following numerical values for E_1 and E_2

R	E_1	E_2
4	0.07	0.320
6	0.061	0.242
8	0.067	0.182

Figure 12 shows that the distributions of U_e calculated from equation (11) using these numerical values are in good agreement with those obtained from measurements. It is noted that E_1 is almost independent of the velocity ratio R as expected, but the cross-jet entrainment coefficient E_2 varies with R in a consistent manner.

Instead of the two entrainment coefficients E_1 and E_2 , Keffer and Baines (reference 11) and Fearn (reference 27) used only one, analogous to E in equation (10). The variation of E with R obtained by Fearn is shown in figure 13. It appears, however, if the normal and parallel flows independently control the entrainment rate as suggested by Kamotani and Greber is correct, the use of two coefficients will be a better approximation. Additional experiments are needed, however, to verify this point and to obtain more data for E_1 and E_2 .

Effects of Jet Orifice Shape and Injection Angle

There are only a limited number of experimental studies on the jet in a crossflow problem with the jet issuing from orifices other than circular in shape at an injection angle not equal to 90° . Wu, McMahon, Mosher and Wright (reference 18) and Mosher (reference 19) have determined jet paths for three orifices (all with the same area) shown in figure 14. Mosher's jet path results are shown in figure 15. It is clear that penetration increases with increasing length-to-width ratio of the jet.

The dependence of the jet path on the injection angle is shown in figure 16 based on Taylor's measurements for a circular orifice (reference 21).

Two experimental studies are currently underway to determine the jet structure issuing from a rectangular orifice (Weston and Thames, reference 28; Fearn, reference 29). In Weston and Thames' experiments, a rectangular orifice with aspect ratio 4 was used and the jet injection ranging from 15° to 105° relative to the tunnel flow. Preliminary results indicate that streamwise rectangular jets penetrate the crossflow more than either the circular or blunt rectangular jets, the latter penetrate the least. In addition, the vortex properties (strength, lateral spacing, and core size) are comparable in magnitude for the circular and streamwise jets with the same exit conditions. Blunt jets have lower vortex strengths and larger values of lateral spacing and core size.

THE SURFACE PRESSURE DISTRIBUTIONS

The static pressure at the surface from which a jet is issued into a crossflow has been measured by many investigators (references 16 to 21). The pattern of constant pressure contours are known to vary considerably with the velocity ratio R , shape of the jet orifice, and injection angle ω . On the other hand, the static pressure distributions over cross sections of the jet at stations sufficiently far from the surface are of a simple pattern. A typical example is shown in figure 17 (reference 26). Evidently, the presence of a turbulent boundary layer at the surface plus the suction action of the jet give rise to complex flow fields and the observed surface pressure patterns.

In order to provide clues for the flow patterns near the surface, many oil film studies have been conducted in recent years. A good example is the classic O.N.E.R.A. photographs cited by Margason (reference 2). Noteworthy is the work by Mosher (reference 19), which covers a wide range of velocity ratios and jet orifice shapes. Revealing oil film patterns suggesting blockage and entrainment effects are of particular interest.

Fearn and Weston's measurements reported in reference 20 provide many useful results on the pressure distribution for a jet issuing normally from a circular orifice at a plate into a subsonic cross flow. Comparisons by Fearn and Weston with the results of other experiments such as Bradbury and Wood's (reference 16) and Mosher's (reference 19) indicate the agreement to be generally good.

In figure 18, the static pressure c_p (defined as $(p - p_\infty)/q_\infty$) contours for $R = 7.0$ and $M_j = 0.94$ are shown as a typical example (reference 20). Three pressure regions can be distinguished. First, there is a positive pressure region upstream of the jet. This is attributed to the blockage of the free stream by the jet. The extent of the region diminishes with an increase of the velocity ratio. A measure of this effect is provided by the distance from the origin to the location F at which $c_p = 0.2$. The variation of the location F with R is given in figure 19.

The second region is the lateral pressure region marked by negative pressure coefficients produced by the acceleration of the free stream around the jet and the jet entrainment. A measure of the size of the region is the location of L at which $c_p = -0.2$ (figure 18). Figure 19 shows that as R increases initially from a value of 2, the size becomes larger approximately in a linear manner, but seems to have reached a limiting dimension as R approaches 10.

The third pressure region is the wake downstream of the jet and the lateral pressure region. It is a fairly narrow region of negative c_p in the free-stream direction, across which the variation of c_p is small. The extent of the wake can be measured by the location W with $c_p = 0.2$ (figure 18). The variation of W with R as can be seen from figure 19 is considerably more remarkable. As R is increased from 3 to 4, W reaches fairly far downstream, but then quickly reduces almost to its original value at R = 3 when R reaches 6. With further increase in R, the location of W moves upstream. The width of the wake appears also to depend on R.

An examination of the pressure distributions indicates that in the lateral region the pressure gradient becomes larger as the jet is approached. In the wake region, the radial pressure gradient is less, and as pointed out by Fearn and Weston the pressure appears to reach a plateau of minimum value close to the jet. This minimum pressure coefficient is about -2 for velocity ratios of 2 to 5, and becomes less negative at larger velocity ratios.

The value of the minimum surface pressure coefficient and its angular location at (or near) the jet orifice are also significant features. The angular location variation of the minimum pressure is shown in figure 20 as a function of R. The minimum pressure coefficient reaches its lowest value of -4.7 at the velocity ratio of 6.1.

To understand certain key features of the pressure patterns, oil film photographs (Mosher, reference 19) have been examined. A typical example is given in figure 21. As generally known, in the dark area directly upstream of the jet the free stream decelerates due to the jet blockage. This is the positive pressure region mentioned previously. Oil film photographs indicate that the size of the region diminishes with increasing R. The displacement of the free stream over the sides of the jet produces the light areas on the oil film photographs indicating negative c_p 's at the surface. Some streamlines, however, lose the forward momentum and move toward the jet, and eventually become entrained. Farther away from the jet, the streamlines subject to less jet action move downstream. The limiting streamline S_{mq} as shown in figure 22 represents the separation line as well as the boundary of the wake near the surface.

The angular location of S determines to a large extent the width of the wake near the surface. Since the surface separation is controlled by the unfavorable pressure gradient, the locations of the separation point and the minimum surface pressure are compared in figure 20. There appears to be a good correlation between the presence of the minimum pressure and the surface separation indicating the interpretation that the wake formation near the surface of the plate as a boundary-layer separation phenomenon over the

surface is a correct one. The problem of wake flow and modeling will be discussed in a later section.

Surface pressure distributions for the three jet orifice shapes shown in figure 14 have been determined by Mosher (reference 19). The results are summarized in figure 23. The values of R covered are 4, 8, 10, and 12. The width-to-length ratio w/l is equal to 0.3 for the streamwise jet, 1.0 for the circular jet, and 3.4 for the blunt jet. Using the circular jet case as the reference, which has been already discussed, the effects of the orifice shapes on the blockage, entrainment, pressure patterns, and others can be analyzed.

Taylor's experiments (reference 21) were conducted to determine the effects on the surface pressure distribution caused by changes in the jet injection angle. As the jet is inclined toward the downstream direction, the low-pressure field becomes more extensive within the wake, but less in the lateral region. Thus, the low-pressure contours assume a "swept-back lobe" appearance. A significant change in the pressure distribution has been found to occur in the wake with a very rapid and nearly complete pressure recovery for an angle of inclination of 30° or more. Taylor also noted a reduction of suction-force coefficient and a downstream movement in the center pressure as the jet inclination increased.

In reviewing our present knowledge of the aerodynamics of a jet in a cross-flow, important gaps appear to exist, although considerable progress has been made in recent years due to mainly experimental work. Additional studies are required for the wake flow, the mechanism of jet entrainment, and the formation of contrarotating vortices among others. The prediction of surface pressure distributions is evidently of primary interest to aerodynamicists. In the next section, current prediction methods will be reviewed.

METHODS OF PREDICTION AND ANALYSIS

Various aerodynamic prediction and analysis methods have been developed and applied successfully to the conventional take-off-and-landing (CTOL) aircraft in the past several decades. These methods have been developed primarily to meet specific needs, and consequently they differ considerably in methodology. With the development of large, high-speed computers, not only is the application of analytical methods such as the lifting surface theories greatly expedited, but the utilization and execution of more advanced techniques; e.g., the panel methods, finite-difference and finite-element methods, become feasible. These methods are generally based, however, on inviscid, potential flow theories, often restricted to incompressible or linearized compressible flows. In some cases, the boundary layer corrections are introduced.

There is no doubt that all these methods for CTOL aircraft are applicable to VSTOL aircraft in conventional flight mode. In the transition or hovering mode, however, the situation is different. For the jet in a crossflow problem, as noted in the preceding section, rotational, viscous and turbulent flow phenomena are significant features.

Semi-empirical prediction methods, which have been effectively applied to many aerodynamic problems for CTOL aircraft, are still in an early stage of development for VSTOL aerodynamics. These methods depend on experiments for the needed empirical constants, which are evidently not yet available for a new type of aircraft such as VSTOL. On the other hand, application of three-dimensional, high Reynolds number, averaged Navier-Stokes equations to VSTOL aerodynamics is still beyond the present computational capabilities. The development of a special-purpose Numerical Aerodynamics Simulation Facility for this purpose is being conducted at the NASA/ARC (reference 30).

Earlier analytical studies on jets were concerned mainly with the determination of the shape of jet axes (see Abromvich in reference 8). An evaluation of these studies has been made by Margason (reference 9). Many of the more recent works in VSTOL aerodynamics were sponsored by the NASA or the U.S. Navy, and reported in the 1969 NASA SYMPOSIUM and 1975 NAVY WORKSHOP. A brief summary of the papers on prediction methods is given in the following. The review paper by Platzler and Margason (reference 3) is an updated summary of the 1975 NAVY WORKSHOP results.

THE 1969 NASA SYMPOSIUM

In the Symposium entitled "Analysis of a Jet in a Subsonic Crosswind" held at NASA/LRC in September 1969, several analytical and numerical prediction methods were presented. Basically, all these methods make use of incompressible potential flow theories; i.e., vortices or doublets to provide the jet blockage, and sinks to simulate the flow entrainment by the jet. The surface pressure is determined from the Bernoulli equation. None of the methods, however, appears to have been developed into practical tools. Consequently, only a few comments will be made on these methods. The exception is Wooler's, which will be reviewed in some detail.

A Blockage-Sink Representation of Jet Interference Effects (Wu and Wright) - A two-dimensional doublet-sink model is proposed. A sink element is placed in the wake region to simulate the combined effect of entrainment by the jet and wake. Comparison of the computed surface pressure distributions with measurements show that the model is applicable to high velocity ratio cases.

Development of an Analytical Model for the Flow of a Jet into a Subsonic Crosswind (Wooler) - Two models are discussed, namely, a vortex model and a sink-doublet model. The sink-doublet model has been further developed under the U.S. Air Force sponsorship (reference 31), and is the most widely used method at the present time.

Numerical Treatment of Line Singularities for Modeling a Jet in a Low-Speed Cross Flow (Skifstad) - The model consists of a pair of contrarotating line vortices and a line sink positioned midway between the line vortices. Both the line vortices and sink are of constant strength. The strength of the vortices are assumed to be given from measurements. The unknowns are the sink strength and the location of the line vortices. The conditions for

determining the unknowns are the line vortices to be force-free. An iterative procedure was suggested for the solution, but no numerical results were given. A formula was derived to show that the entrainment does play a role in the deflection of the jet.

Analytical Description of Jet-Wake Cross Sections for a Jet Normal to a Subsonic Free Stream (Margason) - The analytical work of Chang-Lu was described to show on the basis of a quasi two-dimensional potential flow theory, the rollup of the jet into a pair of contrarotating vortices.

A General Jet Efflux Simulation Model (Heltsley and Kroeger) - A vortex lattice method is applied to a wing and jet configuration. The flow normal to the jet is prescribed to simulate entrainment. The jet cross-sectional shape is assumed to remain constant. Only limited numerical results were presented in the paper.

Calculation of Jet Interference Effects on V/STOL Aircraft by a Nonplaner Potential Flow Method (Rubbert) - The model consists of an empirical jet path, constant cross-sectional shape of the jet, and a surface distribution of doublets and sources on the jet to simulate entrainment. The entrainment velocity on the jet surface is to be obtained from measurements. The dominant flow features were reviewed, but no solution was presented.

THE 1975 NAVY WORKSHOP

In July 1975, the Naval Air Systems Command conducted a workshop to review the status of prediction methods for propulsive flows, and propulsion induced aerodynamic effects for VSTOL aircraft (reference 32). A summary of the prediction methods is given in reference 3.

In the Workshop, Snel presented a prediction method for the jet in a crossflow problem, in which the crossflow may be nonuniform. A method for calculating the surface pressure distribution on the plate based on a diffuse vortex model (developed by Fearn and Weston in reference 13) was outlined by Weston (see also reference 33). These methods will be reviewed and compared with Wooler's.

Three papers were also presented on the aircraft/jet analyses for the transition flight regime. Mineck applied Wooler's prediction method (which includes Wooler's sink-doublet jet model and flow field programs) to the analysis of jet-induced interference effects on a vectored-thrust VSTOL airplane model. Rozendahl, Schmitt and Durando used a vortex lattice method and Wooler's vortex model to calculate the lift induced on a wing by a lift/cruise fan, and compared the results with experiments. A computerized analytical procedure was described by Siclari, Migdal and Palcza (see also reference 34) for the calculation of jet-induced effects on V/STOL aircraft. Empirically determined jet centerline location and empirically prescribed flow entrainment velocity at the jet boundary are needed. All the three papers reported some success of the prediction methods, but some deficiencies were noted.

In the following, three methods for treating the jet in a crossflow problem will be examined; i.e., the methods developed by Wooler, Snel, and Fearn and Weston. These methods are chosen to show several different approaches in terms of the theoretical basis, the assumptions and approximations adopted in the development, and the need for experiments to supply values for parameters or constants in the model. The capabilities and deficiencies of these methods will be discussed.

WOOLER'S METHOD

In Wooler's method (reference 31), the jet is defined by three quantities: the centerline shape, the centerline velocity, and its width d normal to the free-stream direction. The three differential equations for the three quantities are the continuity equation and the momentum equations in the tangential and transverse directions relative to the jet centerline written in the following form:

$$\frac{d}{d\xi}(\rho A_j U_j) = \rho \ell_e U_e \quad (12)$$

$$\rho \frac{d}{d\xi}(A_j U_j^2) = \rho \ell_e U_e U_\infty \cos\theta \quad (13)$$

$$\rho A_j U_j^2 k = \rho \ell_e U_e U_\infty \sin\theta + C_D \cdot \frac{1}{2} \rho U_\infty^2 \sin^2\theta \cdot d \quad (14)$$

where A_j is the cross sectional area, U_j the centerline velocity, and k the curvature of the jet centerline. C_D is the drag coefficient due to the pressure difference on a jet element of unit length, and is taken to be a known empirical constant depending only on the geometry of the jet cross section. The assumption was made that the cross section of the jet sufficiently far downstream ($z \geq 3RD$) is an ellipse with a major-to-minor axis ratio equal to 4. In addition, the entrainment velocity was assumed to have the following form for a jet exhausting normally into a crossflow

$$U_e = \frac{E_c d}{\ell_e} U_\infty \sin\theta + \frac{E_p(U_j - U_\infty \cos\theta)}{1 + E_a(U_\infty/U_j) \sin\theta} \quad (15)$$

where E_c is a cross-jet entrainment coefficient ($E_c d/\ell_e$ is equal to E_2 in equation (11)), and $E_p/(1 + E_a U_\infty \sin\theta/U_j)$ is the parallel-jet entrainment coefficient (equal to E_1). E_a was introduced to allow for the fact that fluids moving away from the jet with momentum not directed toward the jet are less tolerant to entrainment. With the above assumptions, equations (12), (13), and (14) can be solved for the three unknowns U_j , d and z , the vertical coordinate of the jet centerline, as functions of x .

The three entrainment coefficients in equation (15) remain to be determined. Experimental entrainment data for a free jet was used for E_p . Thus E_p was taken to depend on the distance from the jet exit approaching a value

of 0.08 asymptotically in the developed region of the jet. The coefficients E_c and E_a were chosen to give good correlation between the computed and experimentally determined jet centerlines. The final values used were $E_c = 0.45$ and $E_a = 30$.

A cursory examination of the entrainment coefficients from Kamotani and Greber's data (reference 26) and Wooler's results has been made, and the comparison is shown in figure 24. In this figure, Kamotani and Greber's data for E_1 and E_2 are plotted in solid lines. (Note E_1 and E_2 data are available for $R = 4, 6,$ and 8 from reference 25.) The calculated values of E_1 and E_2 based on Wooler's work and some estimates of θ and U_j/U_∞ are given as dashed lines. The estimates are $\theta = 15^\circ, 20^\circ,$ and 25° for $R = 4, 6,$ and $8,$ respectively, and $U_j/U_\infty = R/3$ at $\xi = 10D$. Note the determination of E_1 and E_2 by Kamotani and Greber was made experimentally in a direct way. Wooler's approach requires the solution for the jet centerline involving several approximations and a correlation with experimental data for the jet centerline shape. However, the discrepancies for E_1 and E_2 shown by figure 24 are surprisingly large.

To simulate the blockage effect, a distribution of doublets is placed along the jet centerline. The strength of the doublet along the centerline is obtained from the complex potential of a two-dimensional flow past the ellipse of the jet cross section, and by equating the doublet strength to the coefficient of $(x + iY)^{-1}$ term. The jet entrainment is simulated by a distribution of constant-strength sinks over the surface formed by the centerline and major axis of the jet. The strength of the sinks is determined by a two-dimensional consideration; i.e., $U_e l_e = \bar{m} d$, where \bar{m} is the sink strength, and U_e is given by equation (15). The approximation adopted in this approach of determining the strength of doublets and sinks is the same as the small perturbation theory in aerodynamics. The induced velocity field is calculated by integrating the contributions over the extent of the jet. An image singularity system is used to satisfy the boundary condition at the surface. The pressure distribution is calculated from the Bernoulli equation. Modifications of above analysis to account for arbitrary jet injection angle and multi-jet cases were given in reference 31.

Extensive computations for the surface pressure distributions have been carried out by Wooler (reference 31) and compared with various experiments. Generally, the agreement between the computed results and measured data (reference 35) is good for the regions ahead of the jet. There are significant differences, however, between theory and data in the wake regions behind the jet. A typical example is shown in figure 25 for $R = 8$. Wooler has also indicated that the agreement is better for higher values of R .

As mentioned previously, Mineck (reference 32) made a comparison of Wooler's predicted interference effects on a vectored-thrust VSTOL airplane model in transition flight with test results obtained in the NASA/LRC V/STOL tunnel. He found that: (1) the method predicts the correct trends for the lift interference on the wing although the magnitudes are sometimes incorrect, (2) the method fails to predict the detrimental lift interference on the fuselage with the lift jet, and (3) the jet-induced effects are strongly dependent on the velocity ratio and weakly dependent on angle of attack.

SNEL'S METHOD

The differential equations for the jet centerline used by Snel are the same as Wooler's except the action of the drag force is omitted in the transverse momentum equation. Snel indicated that this approximation gives good results at high velocity ratios. The effect of a non-uniform free stream was considered.

The jet flow is divided into a development region and a fully developed region. In the development region, the mass entrainment is assumed to be ($U_\infty = \text{constant}$)

$$\frac{dm}{d\xi} = \frac{m_0}{DU_{j0}} \left\{ C \frac{\xi}{D} U_\infty \sin\theta + (U_{j0} - U_\infty \cos\theta) E_0 \right\} \quad (16)$$

where C is a constant, and E_0 is equal to

$$E_0 = 0.128 + 0.00118(\xi/D)^2 + 0.000616(\xi/D)^3 \quad (17)$$

E_0 is found to differ from the data of free jet (with no coflow) shown in figure 11, and figure 2 of reference 31.

For the fully developed region, a semi-empirical axial velocity decay relation is derived. No entrainment relation was used. The reason given was that velocity decay is easily measurable, but not the entrainment.

Using the above approach, Snel obtained results for the jet centerlines generally in good agreement with measurements (e.g., reference 11). To calculate the induced flow field, a panel method is used. The normal velocity at the jet surface is determined to satisfy the mass flux along the jet centerline. The calculated static pressure distribution on a flat plate from which a jet issues normally into a crossflow with $R = 8$ is compared with the measured data of reference 35 (figure 26). Again the agreement is not good in the wake region.

FEARN AND WESTON'S METHOD

This method is aimed at the calculation of surface pressure distribution with the flow characteristics of the jet vortices assumed to be known. A description of the method was provided by Weston in reference 32. The details were worked out by Dietz in reference 33. The trajectories and strengths of the vortices are given by the empirical equations (see equations (3) to (6)) chosen to fit experimental data. In the numerical evaluation of the induced velocity field, a series of finite strength straight-line filament vortices are placed along the vortex trajectory, with varying strength according to equation (4). Image vortices are used below the plate to represent the boundary conditions on the plate. A series of sink elements are also placed along the jet centerline to simulate entrainment (reference 33). The induced velocity at the plate surface is the sum of the velocity induced by the vortex and sink elements.

In addition, a wake region is defined by a line through the origin at an angle of 45° to the crossflow direction as its boundary (figure 27). In the wake region, the potential flow calculations are replaced by straight-line extensions at constant x/D of the potential - flow results at the boundary of the wake. Figure 27 shows the comparison of computed surface pressure contours with the measurements by Fearn and Weston (reference 20) for a velocity ratio of 8. The agreement between the computed and measured results is fairly good. This approach is expected to be valid for pressure prediction for velocity ratios greater than 5. At lower velocity ratios, curved lines may be necessary to approximate the shape of the wake pressure contours (reference 33).

This method for pressure prediction has several attractive features, and has been found to yield acceptable results for the case $R = 8$. The assumption that the flow characteristics of the vortices are known, however, is a severe one. At the present time, not sufficient results, either analytical or experimental, are available. On the other hand, Wooler and Snel chose to work with the jet centerline, for which both experimental results and empirical formulas are abundant and fairly well established (see Margason, reference 9).

In addition, in the computation of the induced velocity field by the vortices of varying strength, no consideration was given to the trailing vortices. To be consistent, the use of a vortex lattice method or a horse-shoe vortex system can be implemented, perhaps, without too much additional effort. It appears, therefore, that this method needs further development before it becomes a useful tool.

In summary, rational prediction methods for a jet in a crossflow are available, and can produce, together with other methods of aircraft aerodynamics, reasonably accurate and useful results for VSTOL aircraft in transition flight. As noted already, serious deficiencies still exist. The key problem areas are the wake flow, the entrainment mechanism, and the formation of contrarotating vortices. These are general three-dimensional, turbulent flow problems. It appears that in the VSTOL aerodynamics area, the Numerical Aerodynamics Simulation Facility being developed at the NASA/ARC (reference 30) may prove to be a most useful tool.

CURRENT DEVELOPMENTS IN THE AERODYNAMICS OF A JET IN A CROSSFLOW AND TRANSITION AERODYNAMICS

In addition to the present work, several studies in transition aerodynamics, involving both in-house and contract work, have been undertaken by the NADC. A VSTOL aerodynamics assessment has been recently completed by Walters and Henderson at NADC (reference 36). The ultimate goal is the development of computerized prediction and analysis methods for propulsion induced aerodynamics as contributions to a VSTOL Stability and Control Manual being prepared at NADC (reference 37).

Under contract to NADC, Vought Corporation - Systems Division is to develop a methodology for the prediction of Propulsion Induced Aerodynamics of V/STOL

Aircraft in the Transition and STO Flight Regimes. In the transition regime, the methodology will provide prediction of induced pressure distributions as well as the forces and moments on an aircraft of a general configuration. With interactive graphics capabilities, the methodology will be a unified, computerized package based essentially on the Vought V/STOL Aircraft Propulsive Effects Computer Program (VAPE). The major programs include both the Wooler (reference 31) and Dietz (reference 33) jet models, the Hess panel method for three-dimensional flow (reference 38), and a method to compute the propulsion system inlet mass flow effects. This study will make use of the available computer programs, but suitable improvements and modifications as needed will be performed.

An analytical study on the viscous effects for a turbulent jet in a cross-flow is being conducted under NADC sponsorship by Dr. A. J. Baker of the University of Tennessee, and Computational Mechanics Consultants, Inc. The jet flow will be treated by parabolic Navier-Stokes equations, and a finite-element solution algorithm will be derived to account for the interaction between the inviscid, free-stream potential flow and the viscous turbulent jet. Sufficient progress has been made so far to indicate that useful results will be obtained for the jet entrainment and the origin of contrarotating vortices in the jet. The use of parabolic Navier-Stokes equations will render, however, the wake effects of the jet difficult to treat.

In the area of transition aerodynamics, Neilsen Engineering is contracted with NASA/Ames to develop potential flow solutions to the jet in a crossflow problem (reference 39). Empirical modifications will be introduced in the analysis to account for the viscous effects. Wind tunnel testing will also be conducted in the Ames 7' x 10' Wind Tunnel to study the multi-jet problem.

It is evident that several key aerodynamic problems represent serious stumbling blocks for the development of a prediction methodology in transition aerodynamics. The wake problem is the most prominent one, and is probably the most important source of deficiencies in the present prediction methods. Equally significant is the problem of contrarotating vortices in the jet. Their formation and relationship to the jet entrainment as well as the wake flow are not well understood. To solve these problems, both analytical and experimental studies of a fundamental nature are required. A study recently initiated at the NADC is directed at the origin and formation of contrarotating jet vortices and towards the development of a wake flow model. In the following, some preliminary results from the study will be reported.

FORMATION OF CONTRAROTATING VORTICES

As mentioned in the preceding section, Margason (reference 27) has described Chang-Lu's work in which a quasi, two-dimensional potential flow analysis is used to study the formation of contrarotating vortices in a jet in crossflow. The transverse velocity at the jet exit with a circular orifice (the case studied by Chang-Lu) can be taken to be $2U_{\infty}\sin\alpha$, where α is the angle measured from the forward stagnation point. The circulation is

$$DU_{\infty} \int_0^{\pi} \sin\alpha d\alpha = 2DU_{\infty}$$

Thus, a potential analysis of the rollup will yield the vortex strength of $2DU_\infty$. Measurements by Fearn and Weston (reference 13) show, however, that the value of $\gamma = \Gamma/2U_\infty D$ can reach a value as high as 5 or more for a velocity ratio R of 8 (see figure 8). Although the potential analysis is valuable in proving that the underlying mechanism of the origin of the contrarotating vortices is the action of the crossflow, the formation of the vortices depends also on other factors such as the jet flow, the bending of the jet, and the flow entrainment as discussed in the preceding section.

As the first step of the study on the formation of the vortices, an analysis has been carried out to determine the significance of the jet flow on the development of the vortex strength. To simplify the analysis, the flow is taken to be axially symmetrical about the jet axis. Thus, the bending of the jet is not considered. The action of the crossflow is represented approximately by shear stress at the jet boundary. The purpose of the analysis is to determine the relative significance of the jet flow and the "crossflow shear action" for the vortex strength development.

A momentum-integral method similar to that used by Mager in his study of incompressible, viscous, swirling flows through a nozzle (reference 40) is adopted for the analysis. The flow equations with the boundary layer approximation that the gradients in the axial direction are much smaller than those in the radial direction are

$$\frac{\partial(ur)}{\partial r} + r \frac{\partial w}{\partial z} = 0 \quad (18)$$

$$\frac{v^2}{r} = \frac{1}{2} \frac{\partial p}{\partial r} \quad (19)$$

$$\frac{\partial(uvr^2)}{\partial r} + r^2 \frac{\partial(vw)}{\partial z} = \frac{1}{Re} \frac{\partial}{\partial r} \left[r^2 \left(\frac{\partial v}{\partial r} - \frac{v}{r} \right) \right] \quad (20)$$

$$\frac{\partial(uwr)}{\partial r} + r \frac{\partial w^2}{\partial z} = -\frac{r}{2} \frac{\partial p}{\partial z} + \frac{1}{Re} \frac{\partial}{\partial r} \left(r \frac{\partial w}{\partial r} \right) \quad (21)$$

In the above equations, u , v , and w are the velocity components in the cylindrical coordinate r , ϕ , and z with z along the jet axis. All velocities are made dimensionless with reference to the free stream velocity U_∞ , the pressure to the dynamic pressure $\rho U_\infty^2/2$, and all lengths to the jet orifice radius ($D/2$). The Reynolds number Re is equal to $\rho U_\infty D/2\mu$, where μ is the coefficient of viscosity.

The jet boundary is defined by its radius $r = \delta(z)$. At the boundary,

$$w = W(z), \quad (22)$$

$$v = V(z), \quad (23)$$

$$p = P(z), \quad (24)$$

$$\frac{\partial w}{\partial r} = 0, \quad (25)$$

$$r \frac{\partial}{\partial r} \left(\frac{v}{r} \right) = \tau^*, \quad (26)$$

where τ^* is the dimensionless shear stress ($D\tau/2\mu U_{0j}$). Note the conditions (25) does not imply stress-free at the boundary. Instead of (26), Mager used the condition $\partial(rv)/\partial r = 0$, also not stress-free. In addition, $V(z)\delta(z)$ is not assumed to be independent of z as in Mager's analysis, in order to study the vortex development. On the axis, the boundary conditions are

$$u = v = \frac{\partial w}{\partial r} = 0, \quad r = 0 \quad (27)$$

At the initial station, $z = 0$, the conditions are $u = 0$, and $\delta = \delta_0$. In addition,

$$w = U_{j0}, \quad r \leq \delta_0 \quad (28)$$

$$w = W_0, \quad r \geq \delta_0. \quad (29)$$

The velocity $W(z)$ and the pressure $P(z)$ are assumed to be known. W may be taken as $U_\infty \cos\theta$, where θ is the angle between the vortex curve and the jet axis. The experimental results in references 12 and 14 show that the development of the contrarotating vortices occurs in a core of nearly circular shape with a diameter considerably smaller than the jet diameter (see figure 5). Thus, δ_0 may not be necessarily equal to $D/2$.

Equations (18) and (19) can be used to eliminate u and p from the equations (20) and (21). Integration across the jet yields the following two momentum integrals

$$V\delta \frac{d}{dz} \int_0^\delta r w dr + \frac{\delta^2 \tau^*}{Re} = \frac{d}{dz} \int_0^\delta r^2 v w dr \quad (30)$$

$$\frac{1}{2} \int_0^\delta r \frac{d}{dz} (v^2) dr = I_1 \frac{dW}{dz} + \frac{dI_2}{dz} \quad (31)$$

where

$$I_1 = \int_0^\delta r(w-W) dr$$

$$I_2 = \int_0^\delta r w(w-W) dr$$

Equation (31) shows the dependence of the swirling kinetic energy on the axial motion, and is not of primary concern in the present analysis. Consequently, in

the following, attention will be directed to equation (30), which shows the coupling between the shear and the jet flow; i.e., τ^* and w as well as W .

The velocity profiles for v and w are chosen to be

$$v = V \left\{ 2\chi - 2\chi^2 + \chi^3 - \frac{1}{2} \frac{\tau^* \delta}{V} (\chi - \chi^3) \right\} \quad (32)$$

$$w = W \{ \lambda + (1-\lambda)(6\chi^2 - 8\chi^3 + 3\chi^4) \} \quad (33)$$

where $\chi = r/\delta$. These velocity profiles satisfy all necessary boundary conditions, but not the initial conditions (28) and (29). At $z = 0$, λ assumes the value of 1, and $w = W_0$. Thus, the discontinuity in the velocity at $r = \delta_0$ and $z = 0$ is ignored in the present analysis. The use of the profile (33) for w simplifies considerably the mathematical operations. The approximation involved may not be a serious one as it appears to be in view of the fact that δ_0 may be considerably smaller than $D/2$. It is assumed that W_0 does not vanish in the present analysis.

Substituting (32) and (33) into (30) yields, after appropriate mathematical operations, the solution for $V\delta$ as follows

$$V\delta = \left\{ \int_0^z \frac{F}{A} \exp\left(\int_0^z -\frac{B}{A} dz\right) dz \right\} \exp\left(\int_0^z \frac{B}{A} dz\right) \quad (34)$$

where

$$A = (.2444 + .0222\lambda)W\delta^2 \quad (35)$$

$$B = \frac{d}{dz} \{ (.1556 + .0778\lambda)W\delta^2 \} \quad (36)$$

$$F = \frac{\delta^2 \tau^*}{Re} + \frac{d}{dz} \{ (.0355 + .006116\lambda)W\delta^4 \tau^* \} \quad (37)$$

Equation (34) shows that τ^* plays a key role in the origin of the vortex, but the jet flow is significant for its formation. The function F can be written as

$$F = \frac{\delta^2 \tau}{\rho U_\infty^2} + \frac{d}{dz} \left\{ (.0355 + .006116) W \delta^4 \frac{\tau}{\rho U_\infty^2} \frac{\rho D U_\infty}{2\mu} \right\} \quad (38)$$

The term $\delta^2 \tau$ represents the shear in the form of a torque acting on a jet element of unit length, Thus, except for an amplification factor, the first term in F gives rise to approximately

$$d(V\delta) \sim \frac{\delta^2 \tau}{\rho U_\infty^2} \frac{dz}{W\delta^2} \quad (39)$$

Similarly, the second term in F leads to

$$d(V\delta) \sim d\left(\frac{\delta^2 \tau}{\rho U_\infty^2}\right) + \frac{\delta^2 \tau}{\rho U_\infty^2} d \ln (W\delta^2) \quad (40)$$

The first term in (40) evidently corresponds to the shear effect without the jet flow. The factor W in (39) appears to be simply a time scale. The second term in (40) is, consequently, the major dynamic effect of the jet flow. This result is rather unexpected based on a heuristic reasoning. Equation (38) also suggests that the second term is more effective in the intensification of the vortex at a high Reynolds number $\rho U_\infty D / 2\mu$; i.e., the terms in (40) are more effective than the term in (39).

The velocity profiles (32) and (33) for v and w have been chosen for simplicity in mathematical analysis. As pointed out already, the discontinuity in w at $r = \delta_0$ and $z = 0$ has not been taken into account. The analysis is being extended with an improved w profile with the discontinuity.

In addition, the term $W\delta^2$ is proportional to the mass flow flux of the jet including the flow entrainment. Thus, the second term in F also suggests the importance of properly accounting for the entrainment. Since the present analysis is restricted to laminar flow, an extension to the turbulent case is needed.

To treat realistically the problem of the vortex formation for a jet in a crossflow, the approach adopted in the present analysis (e.g., the assumption of axial symmetry for the flow field) is obviously inadequate. It is necessary to study the bending of the jet, and to determine the action of the crossflow in stretching and tilting of the vorticity field generated by the jet flow. A study of this problem for a jet issuing from an "unskirted" cylindrical pipe has been conducted experimentally by Moussa, Trischka and Eskinazi (reference 41).

THE WAKE OF A JET IN A CROSSFLOW

To determine the jet-induced aerodynamic effects including the surface pressure distribution, it is necessary to account for the wake effects. As mentioned in the preceding section, the wake problem is a key stumbling block for the development of prediction methodology in transition aerodynamics.

Several two-dimensional wake models have been developed for calculating the wake pressure. An example is Parkinson and Jandali's work (reference 42), in which two sources are introduced to simulate the blocking action of the wake. The strength and location of the sources are determined by the location of the "separation points" and the static pressure at these points. The location of separation points and the pressure must be measured. Satisfactory results for the pressure distribution and pressure drag for several two-dimensional bodies have been obtained by Parkinson and Jandali.

To develop an analytical model capable of predicting "nonuniform" pressure distribution in a three-dimensional wake such as that behind a jet in a crossflow is evidently a more difficult problem. In fact, the wake pressure in two-dimensional models presently available is usually taken to be a constant. The action of the jet on the crossflow in the presence of a surface, however, gives rise to complex flow patterns in the vicinity of the surface, and neither a dead-water region nor a single pressure can be considered as a satisfactory assumption. Thus, there is a need to examine the wake flow structure.

An experimental study of the wake flow with measurements of the velocity field in sufficient detail has been reported by Mosher in reference 19. Although the study was conducted for a limited range in the wake, and only for a circular jet orifice and a velocity ratio equal to 8, his results do shed considerable light on the wake problem. A preliminary flow model for the wake, which is similar to Mosher's wake flow pattern (figure 43(c) in reference 19) except the vortices part, is shown in figure 28. This model is still not complete with details, but it does appear to be consistent with results from experiments including oil film studies. Some modifications may be necessary if the velocity ratio and the shape of the jet orifice are changed.

Two essential features shown in figure 28 are of particular interest; i.e., the boundary layer effects in the vicinity of the surface and the development of two concentrated vortices behind the jet in the wake region. As the flow moves over the surface toward the wake, the forward momentum is dissipated giving rise to boundary layer separation along the line Sq . Due to suction action of the jet, there is a turning of the flow toward the jet ahead of the line lmn . Close to the jet, the flow separation is a consequence of the deflection and acceleration of the free-stream flow around the jet producing a low pressure region at the surface. Thus, there is a strong turning of the flow into the jet near and ahead of the point S as can be seen from examining the oil film photograph shown in figure 22.

The wake region near the surface is defined by the line Smq as a boundary, and the flow motion as indicated by the arrow along $m rn$ over the separation bubble will generate a vortex motion. It is possible that the bubble is open so that the flow motion moves downward along tn and feeds into the vortex. The portion of the vortex forward of $m rn$ will turn upward and, strengthened by the action of the free-stream flow along the lateral side, forms the wake vortex. The presence of the wake vortices is apparent from Jordinson's measurements already discussed. The estimated location of the wake vortices is shown in figure 29 based on Jordinson's total pressure plots. At or beyond the station IV, which is above 6 diameters from the exit center, either no vortex or only one vortex can be discerned. It may be added, the lateral spacing of the two vortices as estimated from Jordinson's plots begins with a value of 1.2D for $R = 8$, and becomes smaller downstream with a value of about 1.0D at station III.

According to Dr. F.C. Thames' communication, a wake model with two potential line vortices has been used by him to develop a prediction method for the jet-induced effects, but the details are not yet available.

ENTRAINMENT BY CONTRAROTATING VORTICES

A key element in Wooler's method of prediction (reference 31) is the use of the flow entrainment velocity U_e in the differential equations for the jet centerline. In addition, U_e is assumed to be given by equation (15) with the three entrainment coefficients to be determined empirically. In Kamotani and Greber's experimental work (reference 12), essentially the same form was used in their data analysis for the entrainment velocity.

A comparison (figure 24) of the two entrainment coefficients E_1 and E_2 , the parallel-jet and cross-jet ones, respectively, shows the agreement between Wooler's values and those obtained by Kamotani and Greber are not good. In particular, Kamotani and Greber found that the cross-jet entrainment E_2 varies considerably with the velocity ratio R , while in Wooler's work E_2 remains nearly independent of the velocity ratio. At the present time, the mechanism for the cross-jet entrainment is not yet known. Thus, the dependence of E_2 on R is not certain.

It is possible that the conventional viscous effects may not play a significant role in the cross-jet entrainment. Instead, it is suggested that the underlying mechanism is a "dynamic effect" controlled by the contrarotating vortices in the jet. It is well known that the vortices are accompanied by a strong axial flow along the jet axis. In fact, as mentioned already, with the development of the contrarotating vortices, the maximum velocity shifts from the midplane of the jet to the vortex centers. It is not expected that this shifting is due to viscous effects.

It is suggested that the axial flow is coupled to the dynamic entrainment by the vortices. To test the idea, a two-dimensional analysis has been carried out. Figure 30 shows the streamlines of a uniform flow over a solid body, calculated by placing a vortex at A. The wake is simulated by placing a vortex at B. Next, a sink is also placed at A. Figure 31 shows that a portion of the free stream is entrained into the sink. The key point is that the streamlines shown in figure 31 are open, while those in figure 30 are closed in the neighborhood of A.

The cross-jet velocity is equal to $U_\infty \sin\theta$. If it is assumed that the dynamic entrainment produces the axial flow, and the axial flow is proportional to the vortex strength, the entrainment coefficient E_2 will be expected to vary with the velocity ratio R (for example, figure 24). This is due to the fact that the vortex strength depends on R (figure 8). It also follows that it is more reasonable to use two entrainment coefficients E_1 and E_2 than just one E (discussed earlier in this report).

If the above idea for the dynamic entrainment is correct, the entrainment will be expected to be effective only when the vortex strength increases along the jet axis. In addition, some influence on the wake flow will also be produced depending whether the vortex strength increases or decreases along the jet axis.

Evidently, much remains to be done both analytically and experimentally on the entrainment problem. Experiments will be highly desirable to measure carefully the streamlines of the flow around the jet to determine their shape — open or closed. Measurements for the entrainment velocity and its correlation with the vortex strength for various velocity ratios will be valuable.

CONCLUDING REMARKS

It is well known that VSTOL aircraft technology has many unique aerodynamic features in the transition flight regime, and it is to these features

that the present study is directed. A key element of transition aerodynamics is the problem of a jet in a crossflow. Experimental results for this problem on the jet flow structure including the contrarotating vortices, the jet entrainment, and the wake have been reviewed and analyzed. Some gaps in the present knowledge of the phenomena have been discussed, and additional experimental studies have been suggested in order to fully understand them.

The key problem areas are the flow structure near the jet exit, the entrainment mechanism of the cross-jet flow, and the wake flow near the surface from which the jet is issued. In addition, the role of the contrarotating vortices in the jet entrainment process needs to be determined.

In reviewing the current status in the development of methods of prediction and analysis, several methods; e.g., Wooler, Snel, and Fearn and Weston, are found to be capable of providing reasonably accurate aerodynamic predictions. However, some deficiencies have also been noted, and an attempt has been made to identify the sources of these deficiencies. It is apparent that in nearly all these methods, although they differ somewhat in their physical bases, the major deficiencies lie in the lack of an adequate wake model, and of an understanding of the entrainment mechanism. Both experimental and analytical studies of a fundamental nature are considered as necessary.

Current works in industry and government agencies in transition aerodynamics have been briefly reviewed in the present work. Some preliminary results from a study on the formation of contrarotating vortices and wake modeling have been described. The study, being conducted by the present writer, is still in progress. The preliminary results indicate that the study is a promising one, and additional results will be reported later.

REFERENCES

1. J. Williams and M. N. Wood, Aerodynamic Interference Effects With Jet-Lift V/STOL Aircraft Under Static and Forward-Speed Conditions, TR 66403, Roayl Aircraft Establishment, 1966.
2. R. J. Margason, Review of Propulsion Induced Effects on Aerodynamics of Jet V/STOL Aircraft, NASA TN D-5617, 1970.
3. M. F. Platzer and R. J. Margason, Prediction Methods for Jet V/STOL Propulsion Aerodynamics, Journal of Aircraft, Volume 15, pp. 69-77, 1978.
4. A. W. Carter, Effects of Jet-Exhaust Location on the Longitudinal Aerodynamic Characteristics of a Jet VSTOL Model, NASA TN D-5333, 1969.
5. M. M. Winston, Propulsion Induced Aerodynamic Interference Effects on Jet-Lift VTOL Aircraft, Proceedings of NAVAIR Workshop on Prediction Methods for Jet V/STOL Propulsion Aerodynamics, Volume II, 1975.
6. R. E. Mineck, Comparison of Theoretical and Experimental Interferences on a Jet VTOL Aircraft Model, Proceedings of NAVAIR Workshop on Prediction Methods for Jet V/STOL Propulsion Aerodynamics, Volume II, 1975.

7. J. G. Skifstad, Aerodynamics of Jets Pertinent to VTOL Aircraft, US AFAPL-TR-69-28, 1969.
8. G. N. Abramovich, The Theory of Turbulent Jets, The MIT Press, Cambridge, Mass., 1963.
9. R. J. Margason, The Path of a Jet Directed at Large Angles to a Subsonic Free Stream, NASA TN D-4919, 1968.
10. R. Jordinson, Flow in a Jet Directed Normal to the Wind, R and M 3074, Aeronautical Research Council, Great Britain, 1956.
11. J. F. Keffer and W. D. Baines, The Round Turbulent Jet in a Cross-Wind, Journal of Fluid Mechanics, Volume 15, pp. 481-496, 1963.
12. Y. Kamotani and I. Greber, Experiments in a Turbulent Jet in a Cross Flow, AIAA Journal, Volume 10, pp. 1425-1429, 1972.
13. R. Fearn and R. P. Weston, Vorticity Associated With a Jet in a Cross Flow, AIAA Journal, Volume 12, pp. 1666-1671, 1974.
14. R. L. Fearn and R. P. Weston, Induced Velocity Field of a Jet in a Cross Flow, NASA Technical Paper 1087, 1978.
15. D. Antani, An Experimental Investigation of the Vortices and the Wake Associated with a Jet in Crossflow, Ph.D. Thesis, Georgia Institute of Technology, 1977.
16. L. J. S. Bradbury and M. N. Wood, The Static Pressure Distribution Around a Circular Jet Exhausting Normally From a Plane Wall Into an Airstream, Technical Note Aero 2978, Royal Aircraft Establishment, Great Britain, 1964.
17. R. D. Vogler, Interference Effects of Single and Multiple Round or Slotted Jets on a VTOL Configuration in Transition, NASA TN D-2380, 1964.
18. J. C. Wu, H. M. McMahon, D. K. Mosher, and M. A. Wright, Experimental and Analytical Investigation of Jets Exhausting Into a Deflecting Stream, Journal of Aircraft, Volume 7, pp. 44-51, 1970.
19. D. K. Mosher, An Experimental Investigation of a Turbulent Jet in a Cross Flow, Ph.D. Thesis, Georgia Institute of Technology, 1970.
20. R. L. Fearn and R. P. Weston, Induced Pressure Distribution of a Jet in a Crossflow, NASA TN D-7916, 1975.
21. P. Taylor, An Investigation of an Inclined Jet in a Crosswind, The Aeronautical Quarterly, Volume 28, pp. 51-58, 1977.
22. P. T. Wooler, G. H. Burghart, and J. T. Gallagher, Pressure Distribution on a Rectangular Wing With a Jet Exhausting Normally Into an Airstream, Journal of Aircraft, Volume 4, pp. 537-543, 1967.
23. W. Mikolowsky and H. McMahon, An Experimental Investigation of a Jet Issuing From a Wing in Crossflow, Journal of Aircraft, Volume 10, pp. 546-553, 1973.
24. D. S. Outerhout, An Experimental Investigation on Jet Emitting from a Body of Revolution Into a Subsonic Free Stream, NASA CR-2089, 1972.

25. Y. Kamotani and I. Greber, Experiments on a Turbulent Jet in a Cross Flow, Report FTAS/TR71-62, Case Western Reserve University (NASA CR-72893), 1971.
26. B. G. Newman, The Prediction of Turbulent Jets and Wall Jets, Canadian Aeronautics and Space Journal, Volume 15, pp. 288-305, 1969.
27. Analysis of a Jet in a Subsonic Crosswind, NASA SP-218, 1969.
28. R. P. Weston and F. C. Thames, Development of an Analytical Model for Rectangular Jet Flow Issuing Into a Crosswind, NASA/Langley Research Review, April 1978.
29. Study being conducted by Dr. R. Fearn under NASA/Langley sponsorship.
30. Future Computer Requirements for Computational Aerodynamics, NASA Conference Publication 2032, 1978.
31. P. T. Wooler, H. C. Kao, M. F. Schwendemann, H. R. Wasson, and H. Ziegler, V/STOL Aircraft Aerodynamic Prediction Methods Investigation, Air Force AFFDL-TR-72-26, 1972.
32. Prediction Methods for Jet V/STOL Propulsion Aerodynamics, Proceedings of Naval Air Systems Command Workshop, 1975.
33. W. E. Dietz, Jr., A Method for Calculating the Induced Pressure Distribution Associated With a Jet in a Crossflow, M.S. Thesis, University of Florida, 1975.
34. M. J. Siclari, J. Barche and D. Migdal, V/STOL Aircraft Prediction Technique Development for Jet-Induced Effects, PDR-623-18, Grumman Aerospace Corporation, 1975.
35. L. B. Fricke, P. T. Wooler and H. Ziegler, A Wind Tunnel Investigation of Jets Exhausting Into a Crossflow, Air Force AFFDL-TR-50-154, 1970.
36. M. Walters and C. Henderson, V/STOL Aerodynamics Technology Assessment, NAVAIRDEVCON Report No. NADC-77272-60, 1978.
37. V/STOL Stability and Control Manual Development, Program Element No. 62241N, Naval Air Development Center, August 1, 1978.
38. J. L. Hess and D. P. Mack, Calculation of Potential Flow About Arbitrary Three-Dimensional Lifting Bodies, McDonnell Douglas Corporation, Report J5679, 1972.
39. NASA/Ames V/STOL Fighter/Attack Status Report, V/STOL Systems Office, September 1978.
40. A. Mager, Incompressible, Viscous, Swirling Flow Through a Nozzle, AIAA Journal, Volume 9, pp. 649-655, 1971.
41. A. M. Moussa, J. W. Trischka and S. Eskinazi, The Near Field in the Mixing of a Round Jet With a Cross-Stream, Journal of Fluid Mechanics, Volume 80, pp. 49-80, 1977.
42. G. V. Parkinson and T. Jandali, A Wake Source Model for Bluff Body Potential Flow, Journal of Fluid Mechanics, Volume 40, pp. 577-594, 1970.

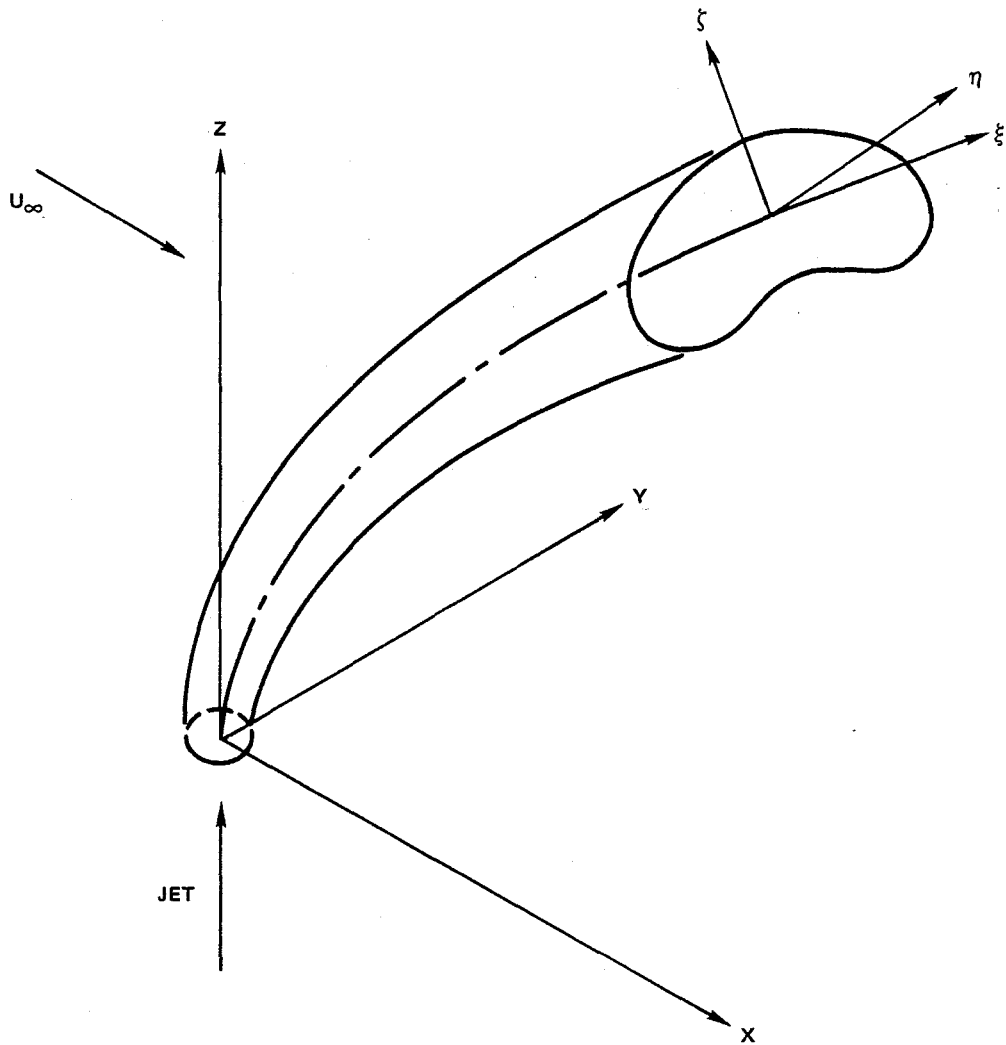


FIGURE 1 - A Jet in a Crossflow

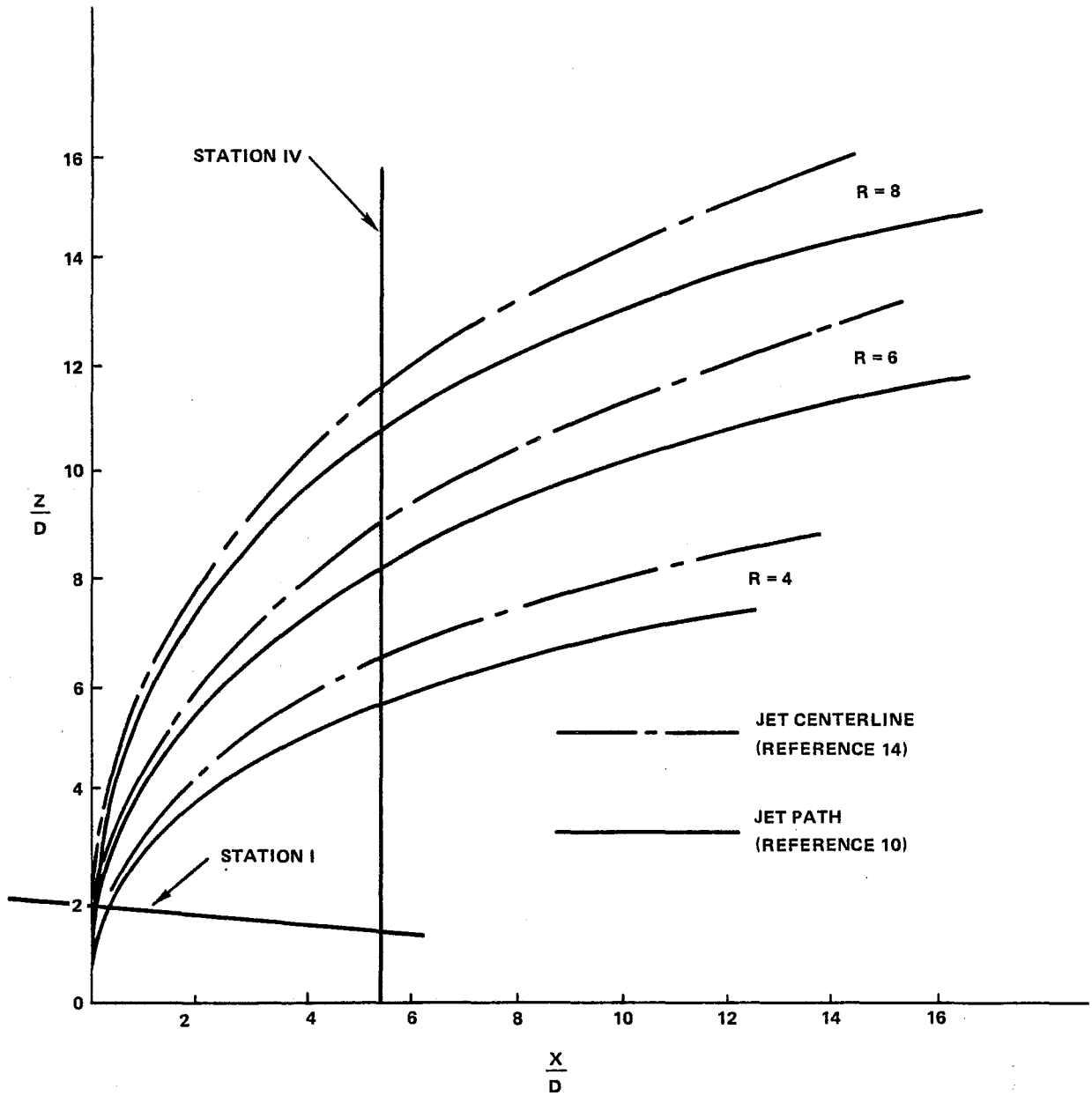


FIGURE 2 - Jet Path and Centerline for Various Velocity Ratios

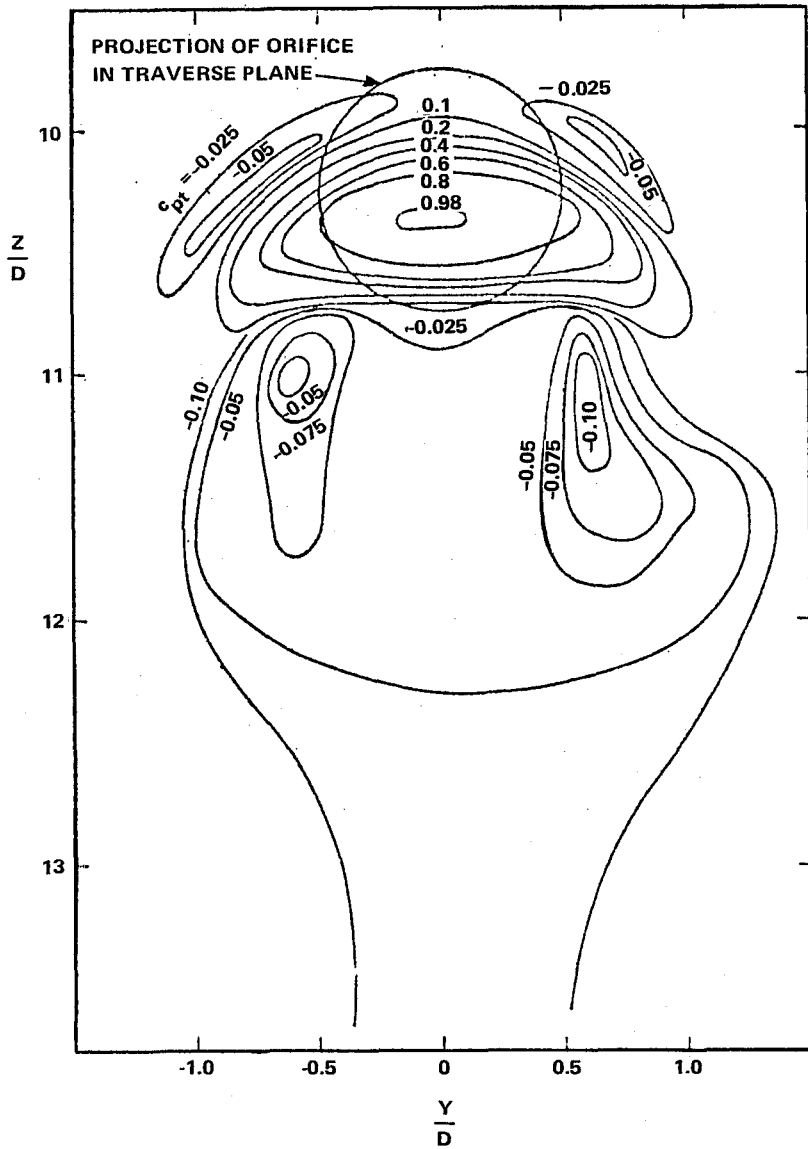


FIGURE 3 - Total Pressure Contours at Station I, R = 6

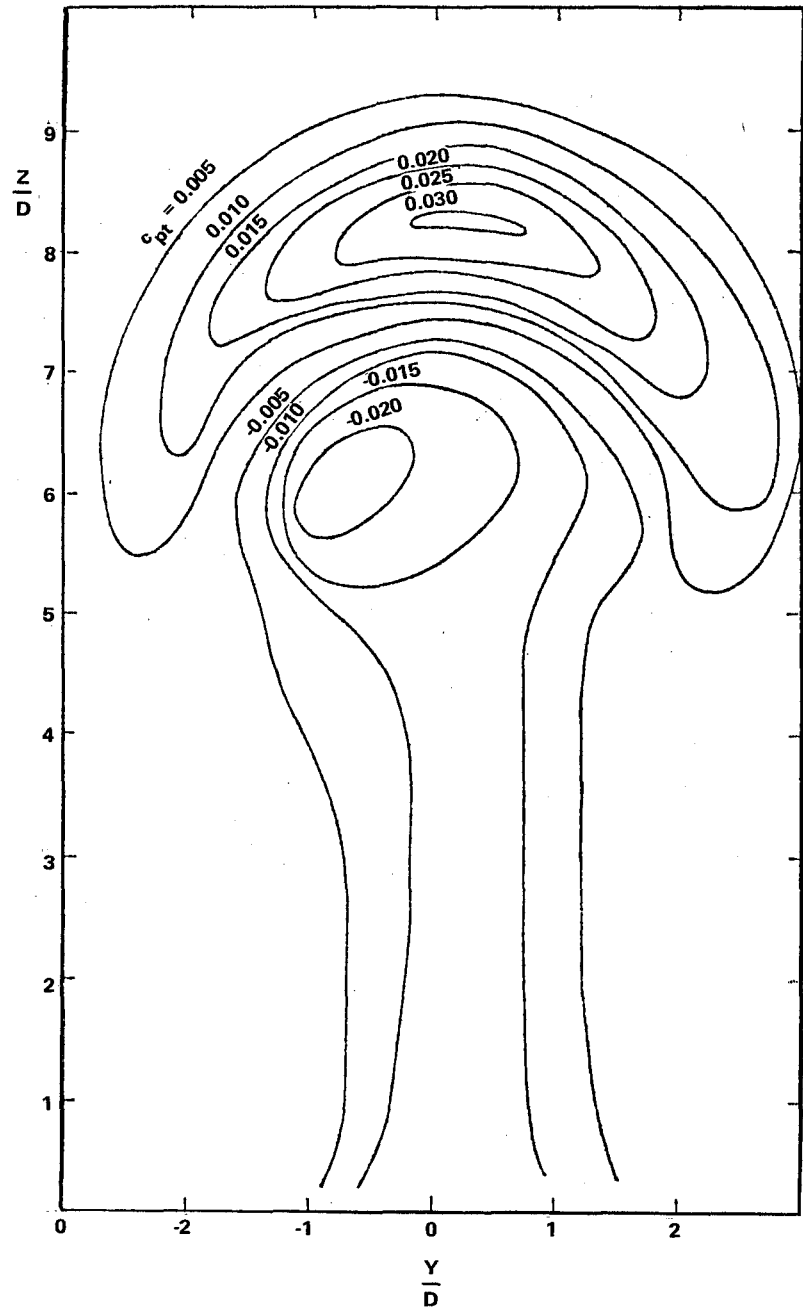


FIGURE 4 - Total Pressure Contours at Station IV, R = 6

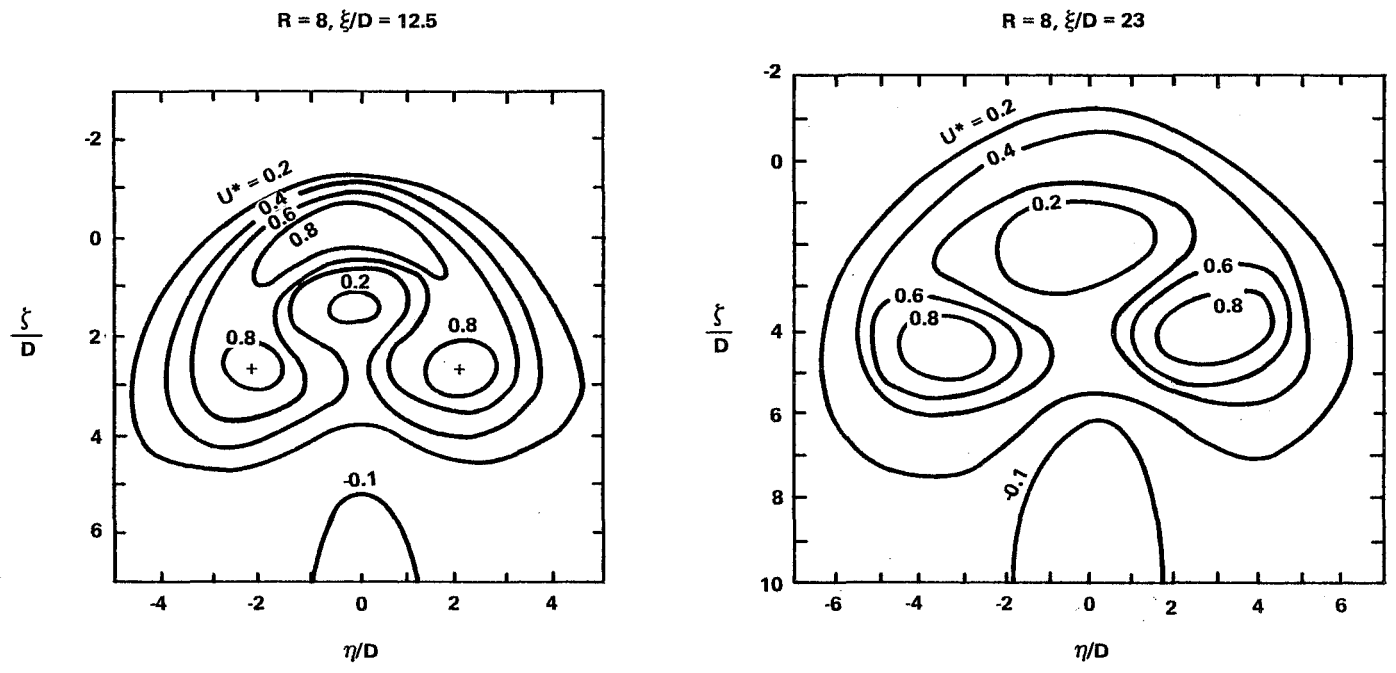


FIGURE 5 - Contours of Constant Velocity, $R = 8$, $\xi/D = 12.5$ and 23

R = 8, $\xi/D = 12.5$

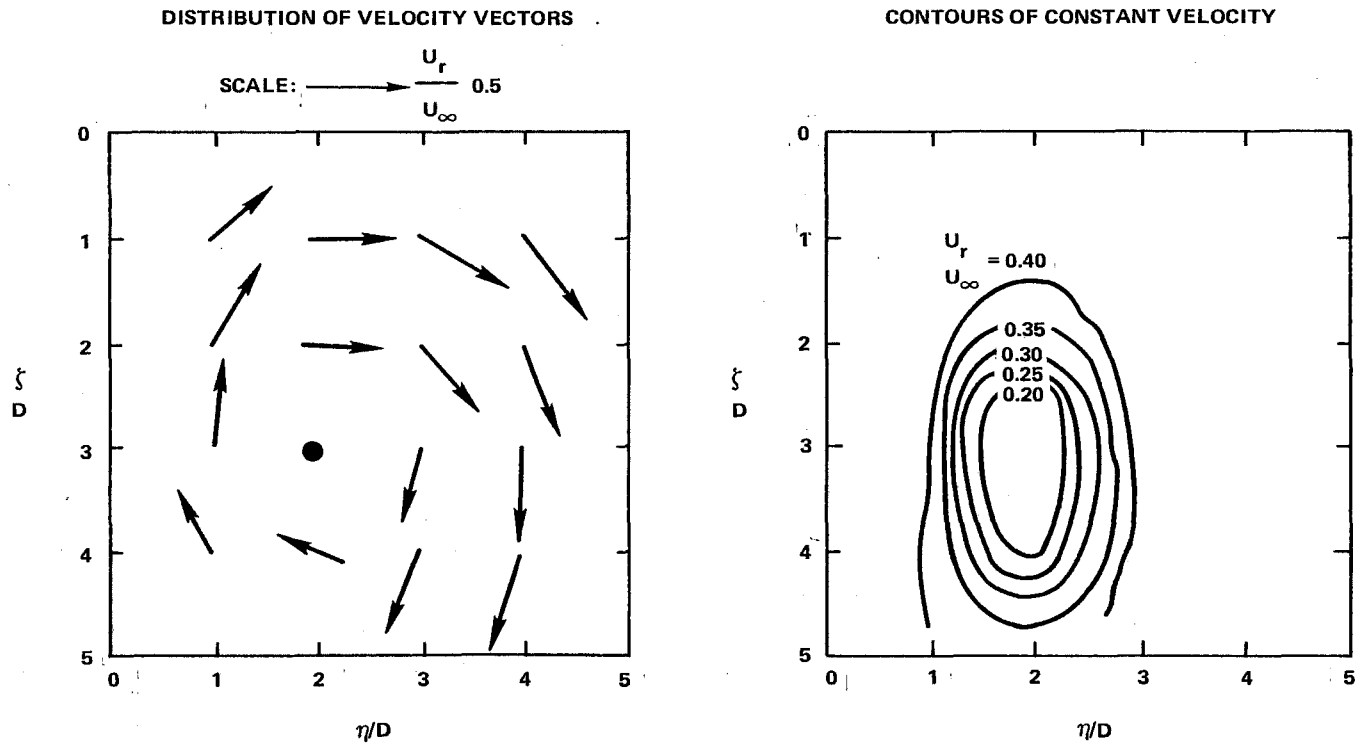


FIGURE 6 - Rotational Velocity Field in Vortex Region, R = 8 and $\xi/D = 12.5$

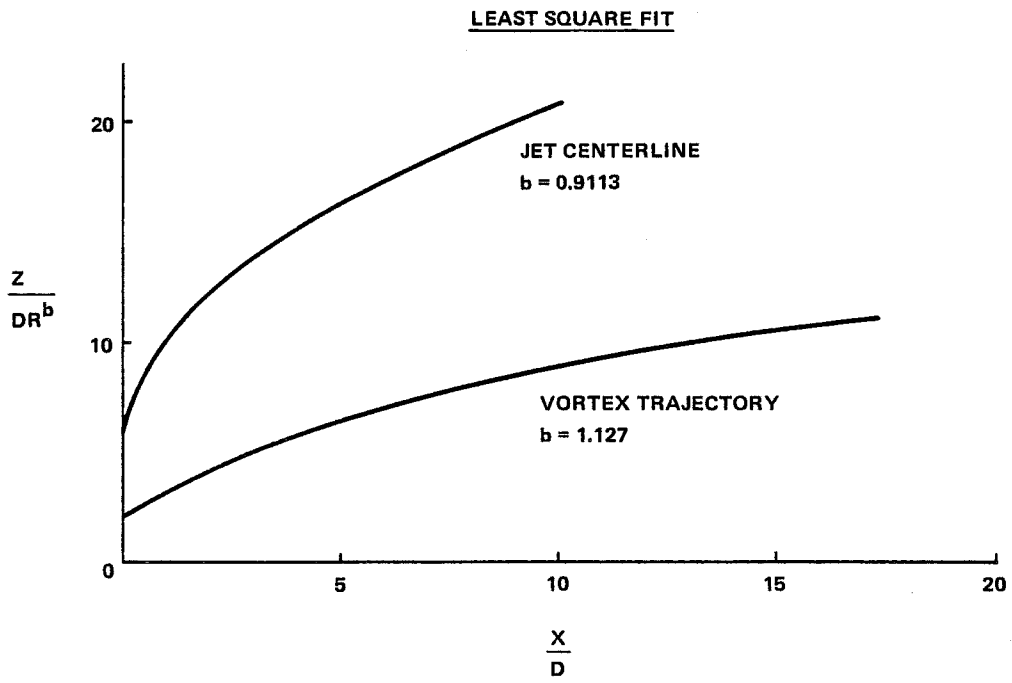


FIGURE 7 - Jet Centerline and Vortex Trajectory

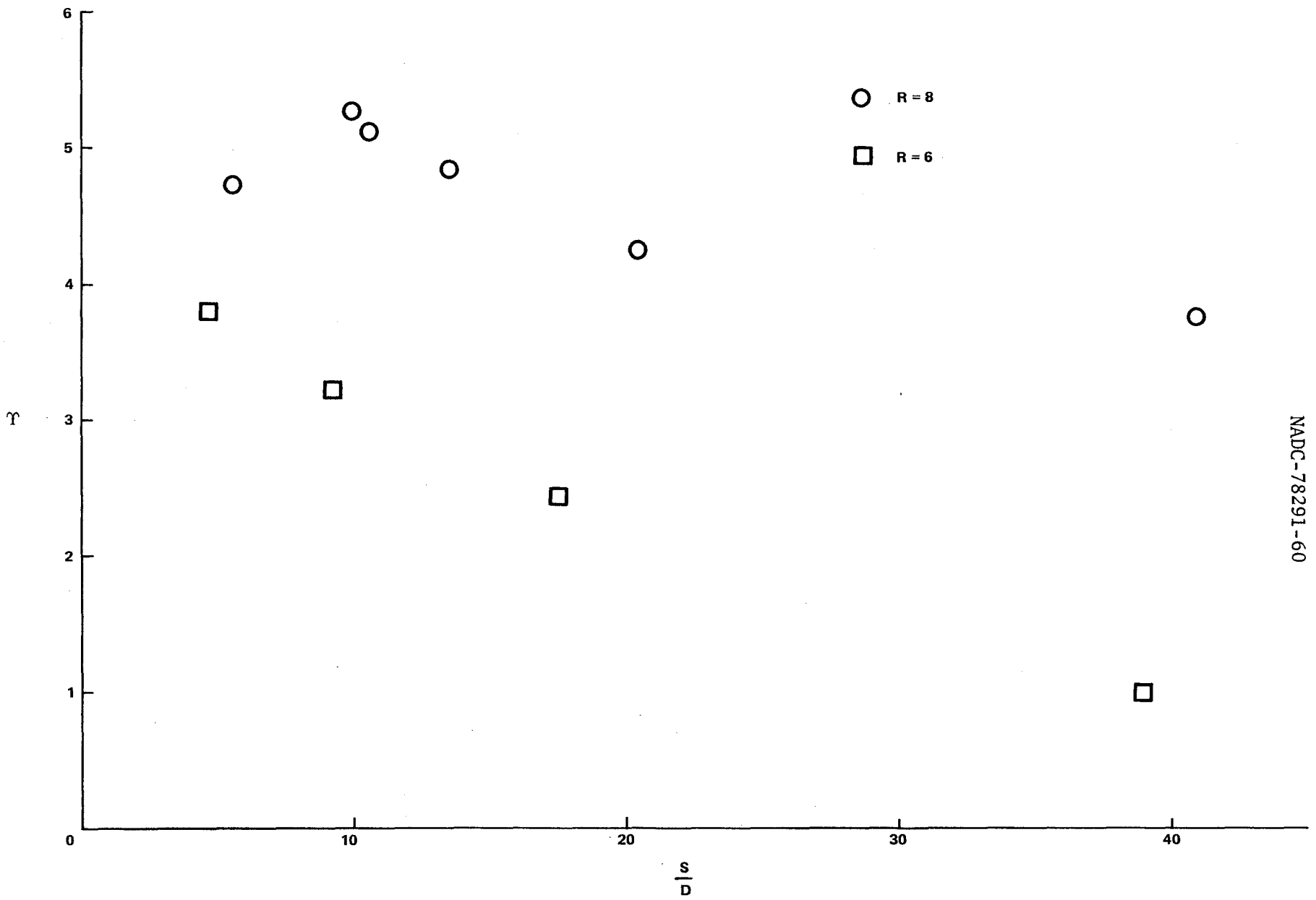


FIGURE 8 - Vortex Strength Distributions (Fearn and Weston, reference 13)

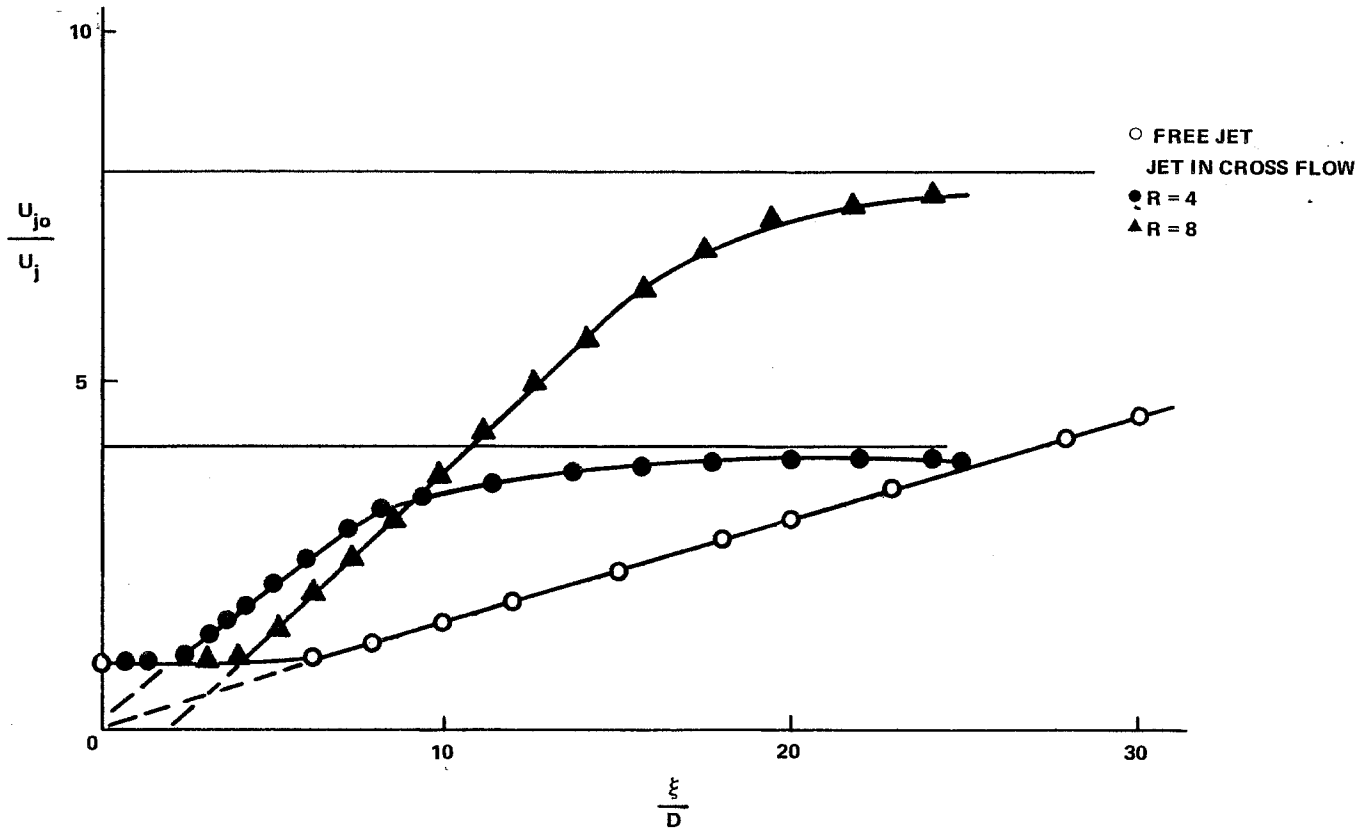


FIGURE 9 - Distribution of Velocity Along the Jet Centerline

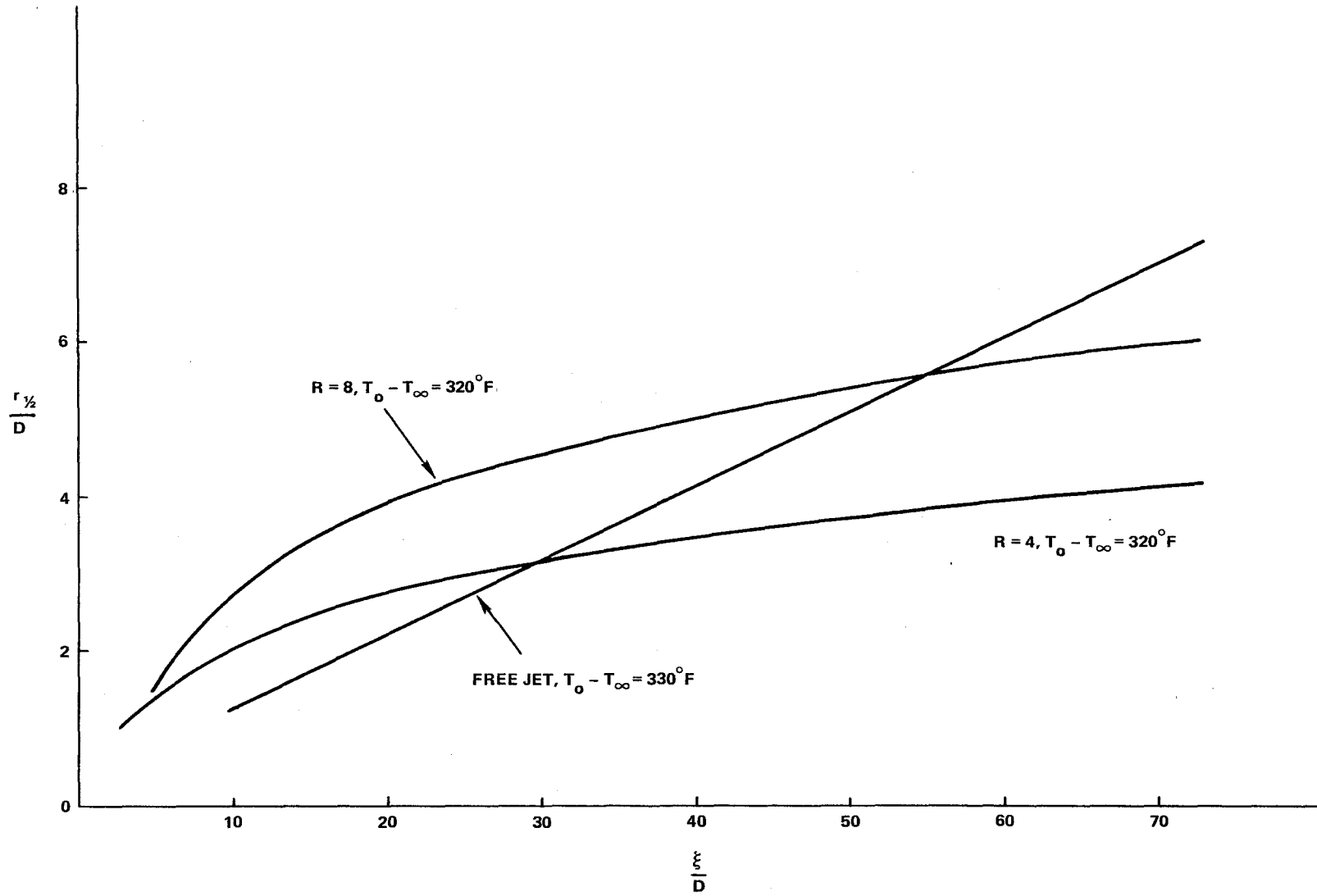


FIGURE 10 - Lateral Spread of Heated Jet

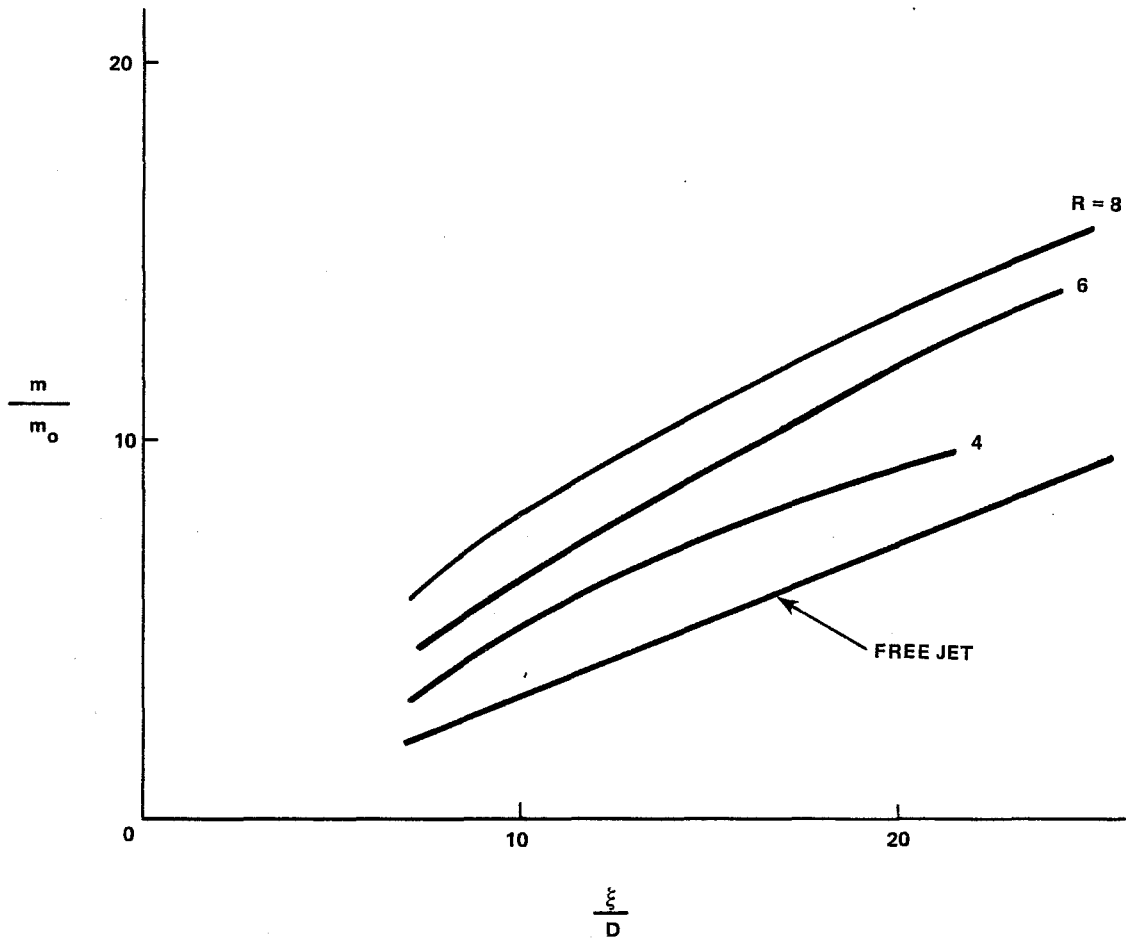


FIGURE 11 - Mass Flux Distributions

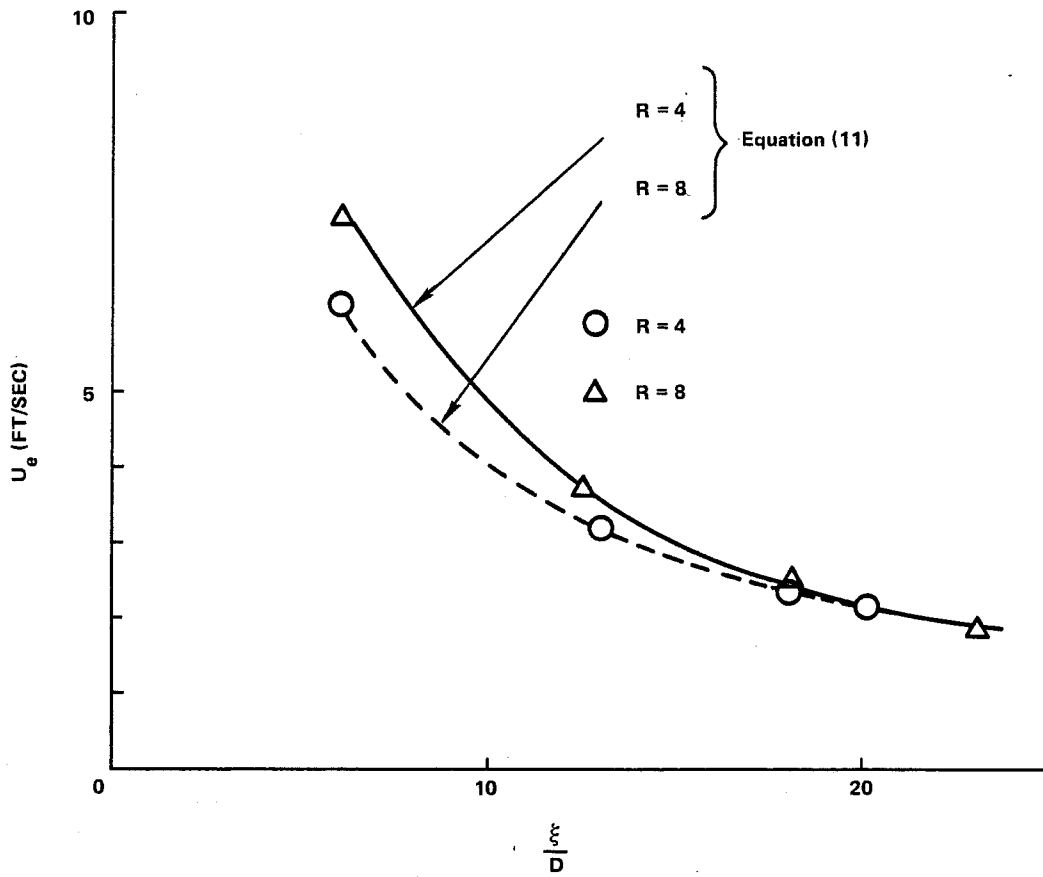


FIGURE 12 - Entrainment Velocity Distributions

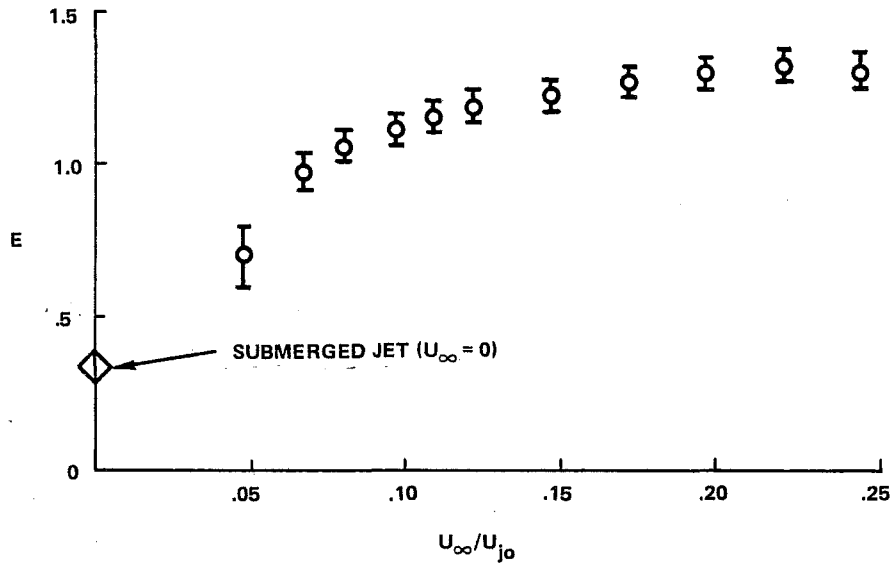


FIGURE 13 - Variation of Entrainment With the Velocity Ratio U_∞/U_{j0} (reference 27)

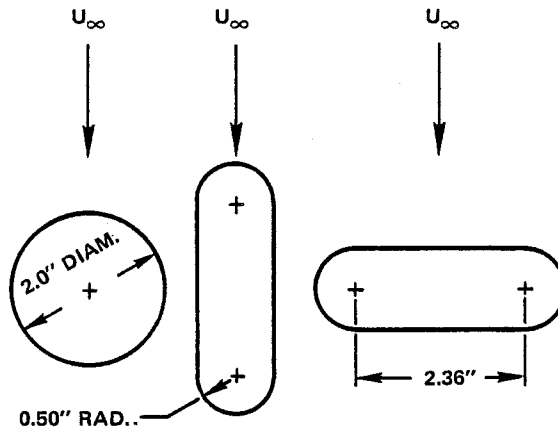


FIGURE 14 - Jet Orifice Configurations (reference 19)

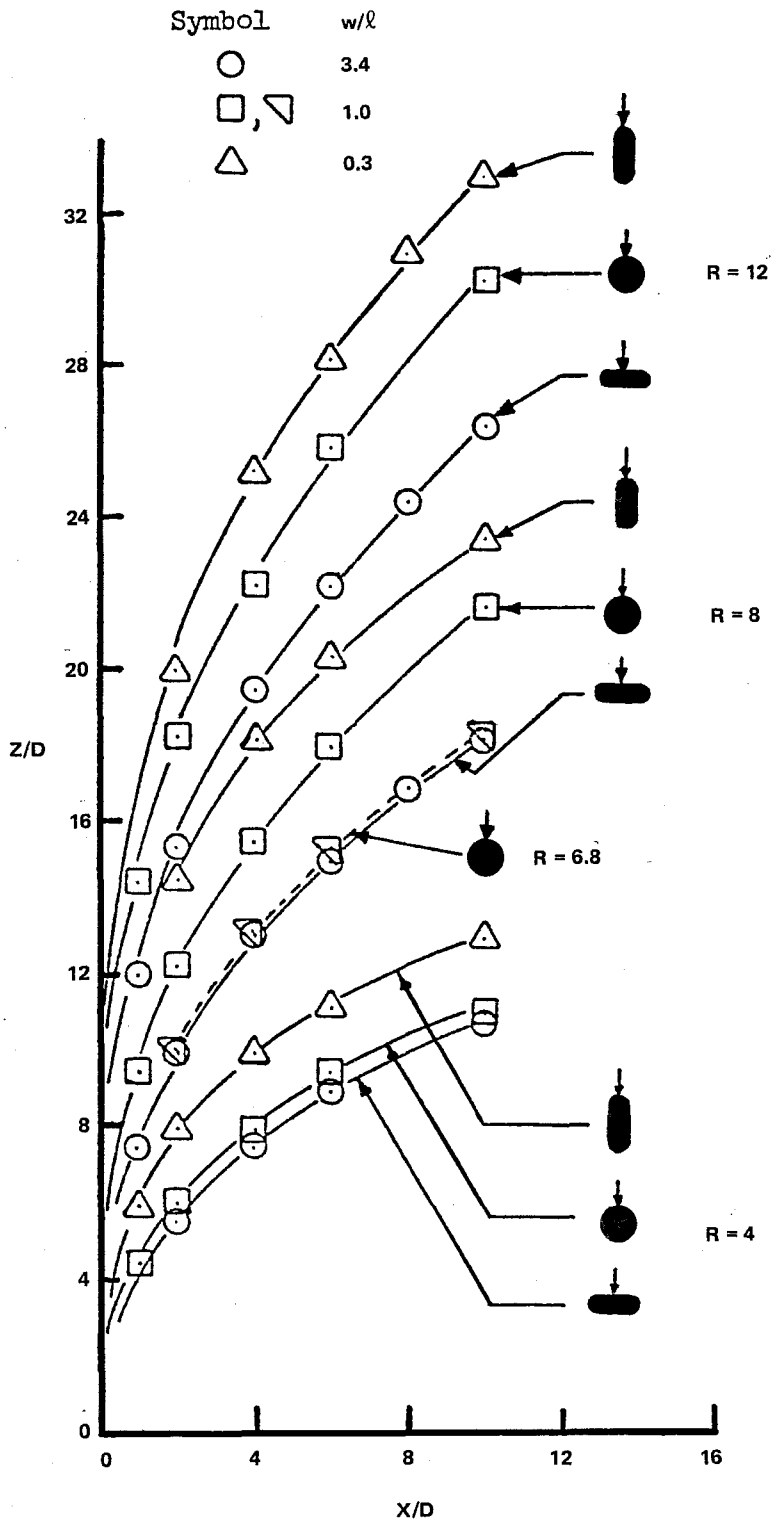


FIGURE 15 - Jet Paths With Injection Angle $\omega = 90^\circ$

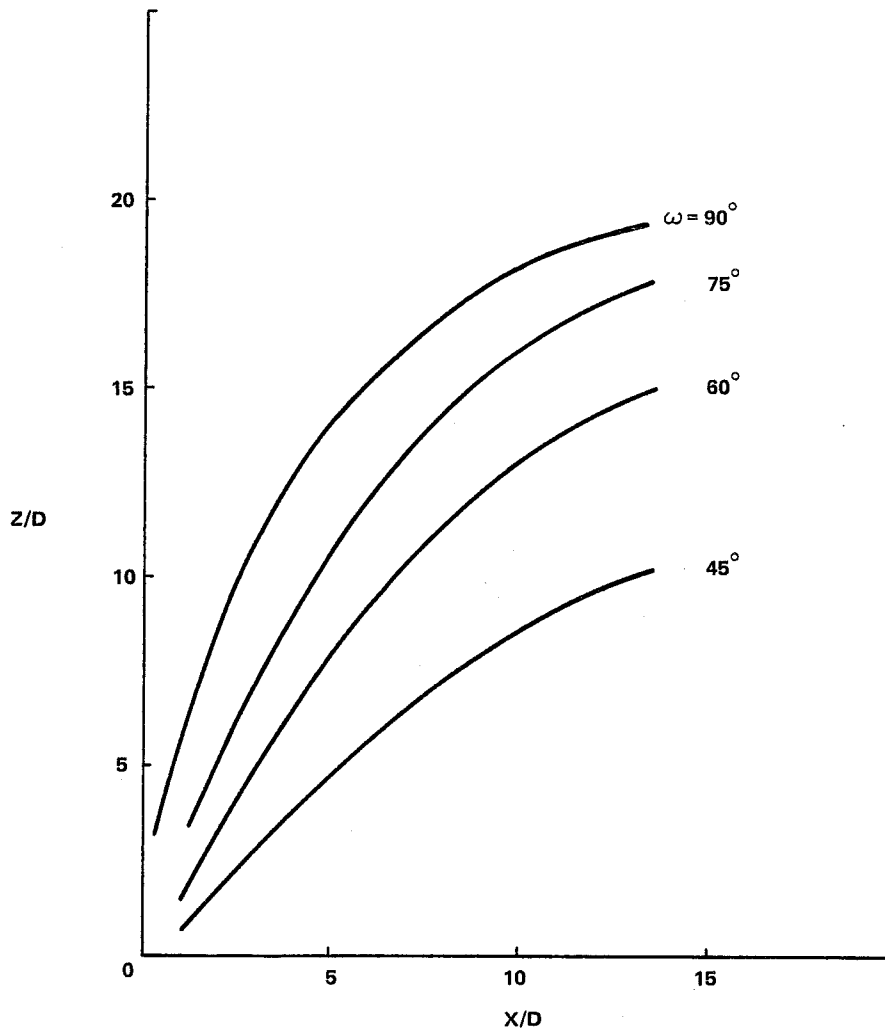


FIGURE 16 - Estimated Jet Paths Based on Taylor's Measurements (reference 21) for Various Injection Angles

R = 4, X/D = 15

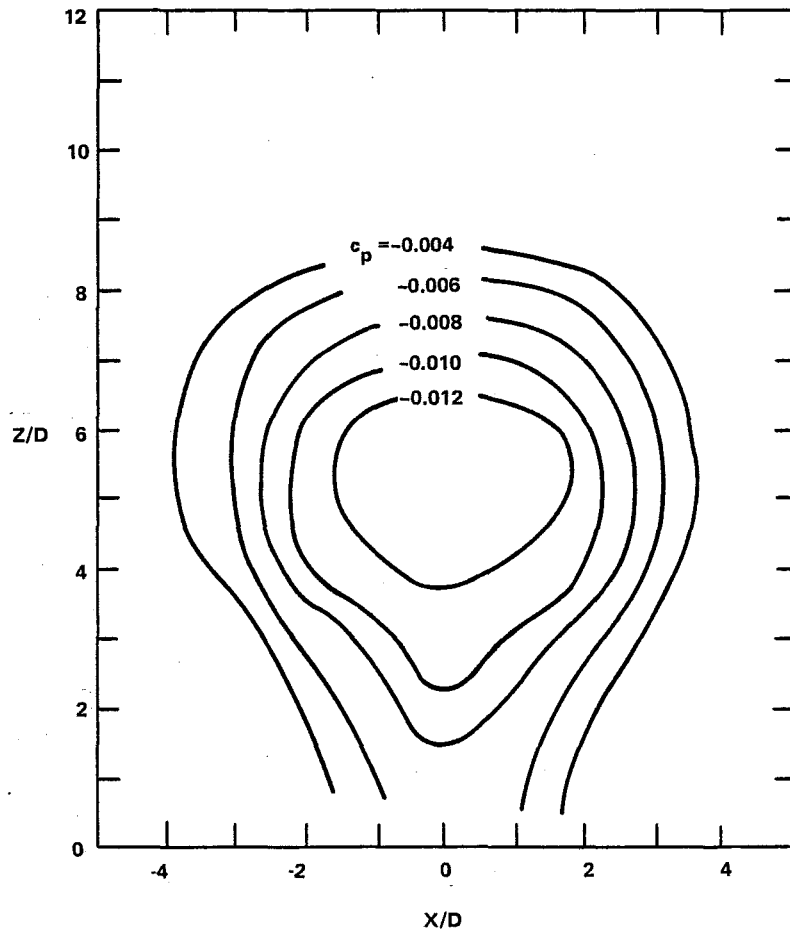


FIGURE 17 - Static Pressure Distribution

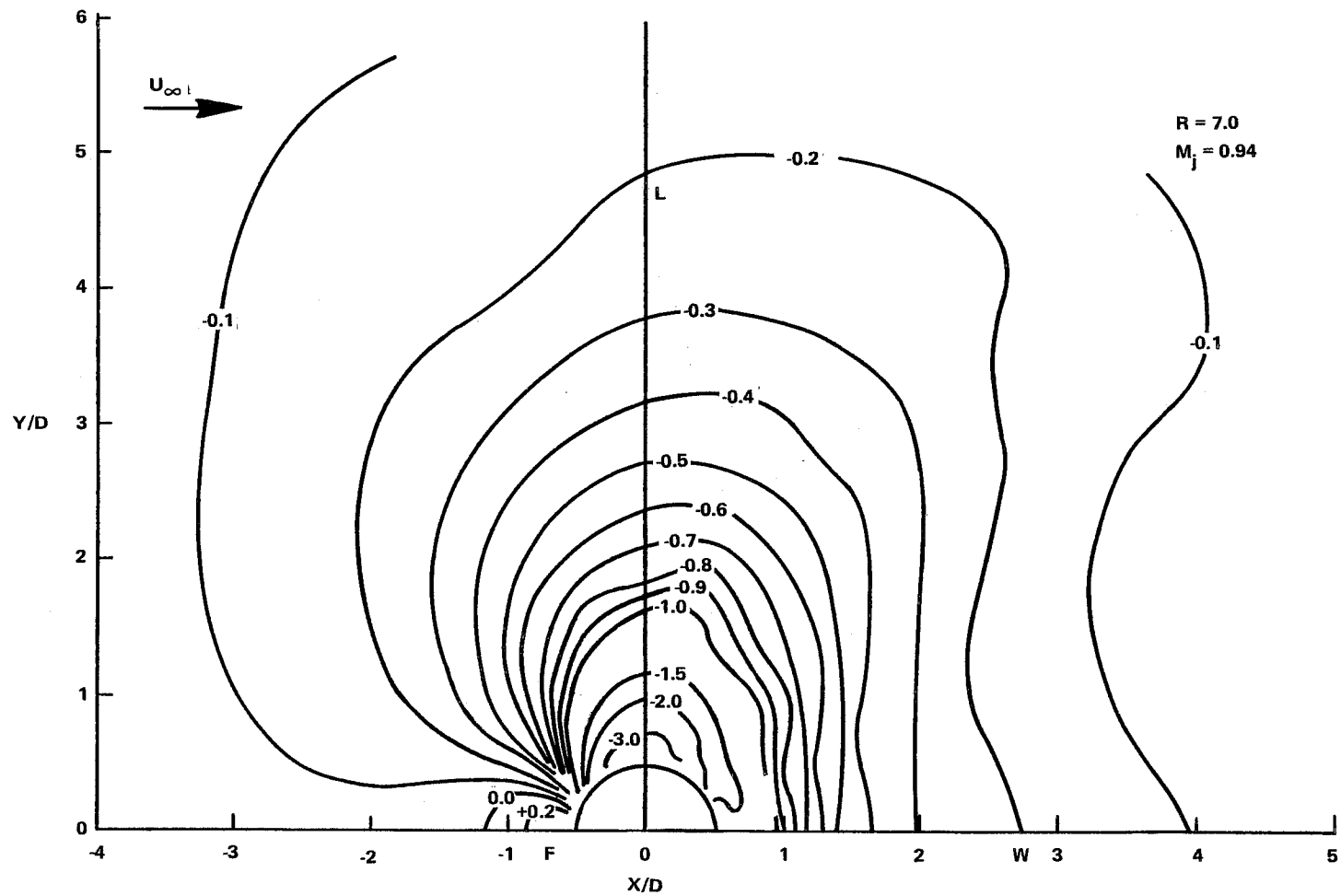


FIGURE 18 - Contours of Constant c_p , $R = 7.0$

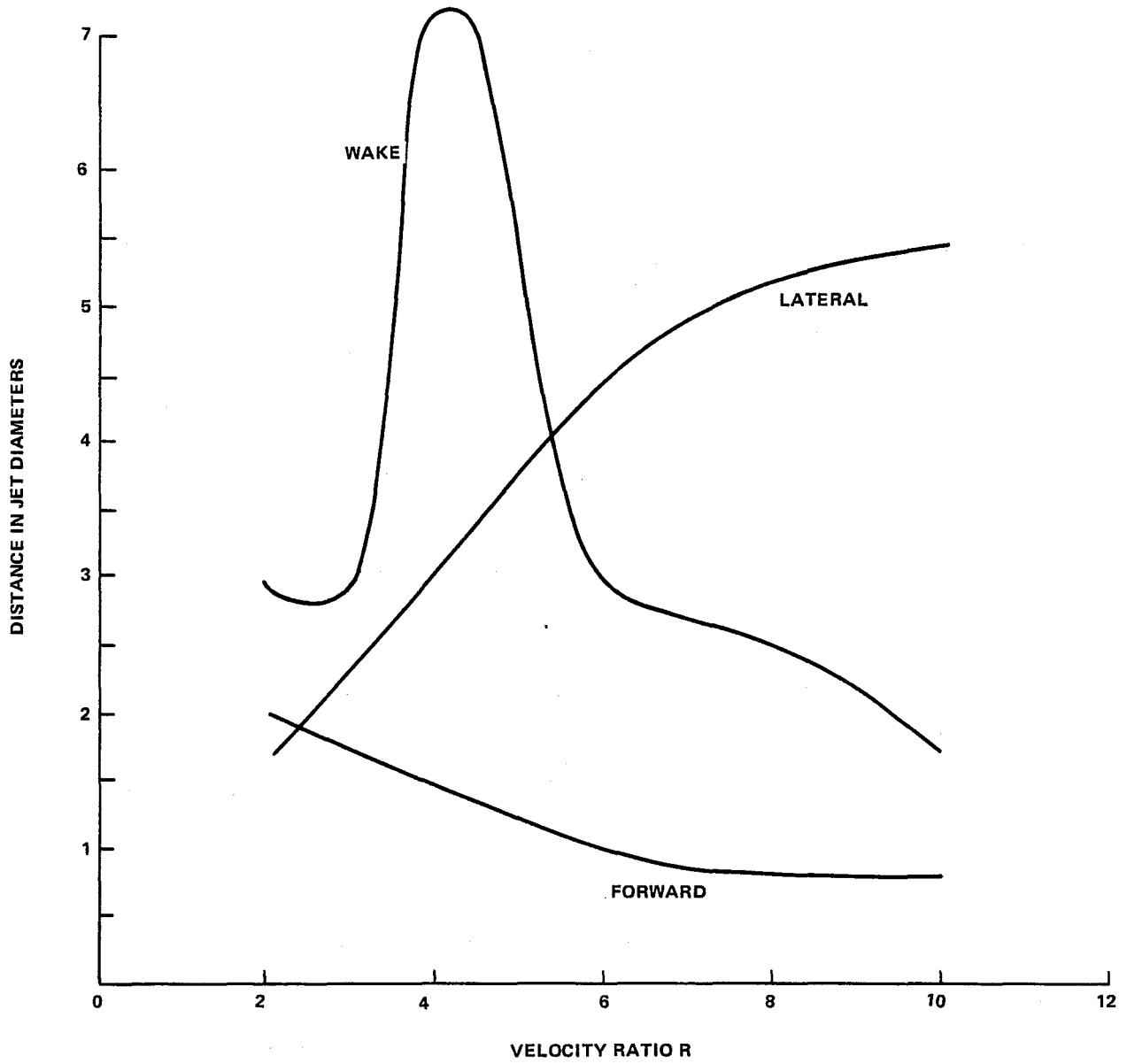


FIGURE 19 - Estimates of the Size of the Three Regions Versus the Velocity Ratio R

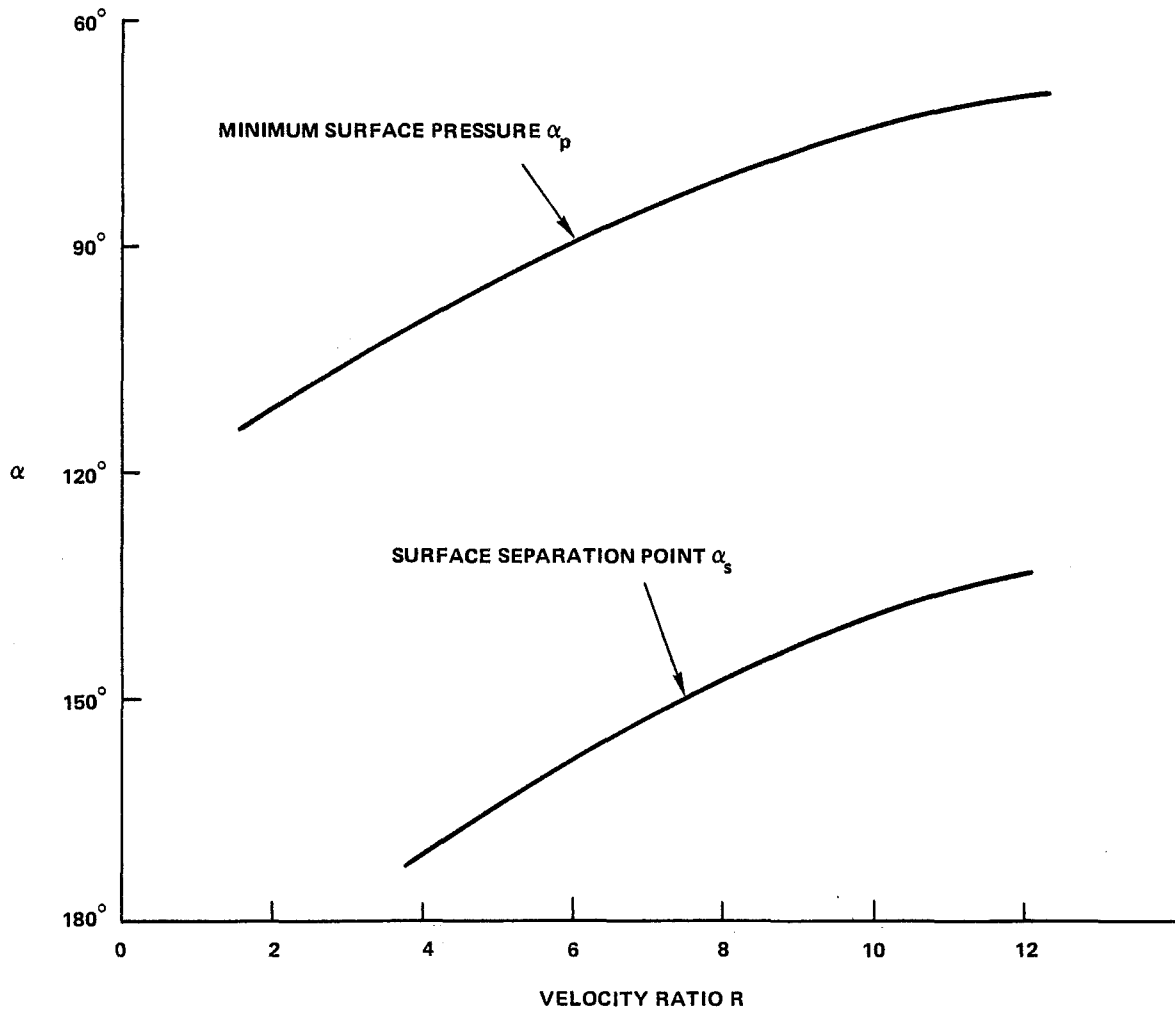


FIGURE 20 - Locations of Minimum Pressure Point and Separation Point Versus the Velocity Ratio R



FIGURE 21 - Oil Film Photograph for $w/\ell = 1.0$, $R = 12$ (reference 19)

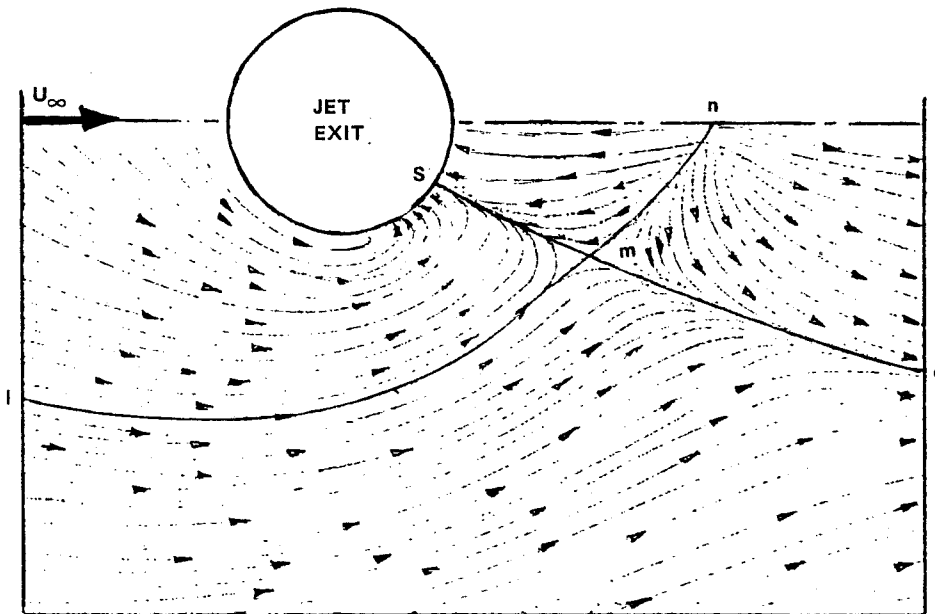


FIGURE 22 - Oil Film Pattern on the Plate From Which a Jet is Issued Into a Crossflow

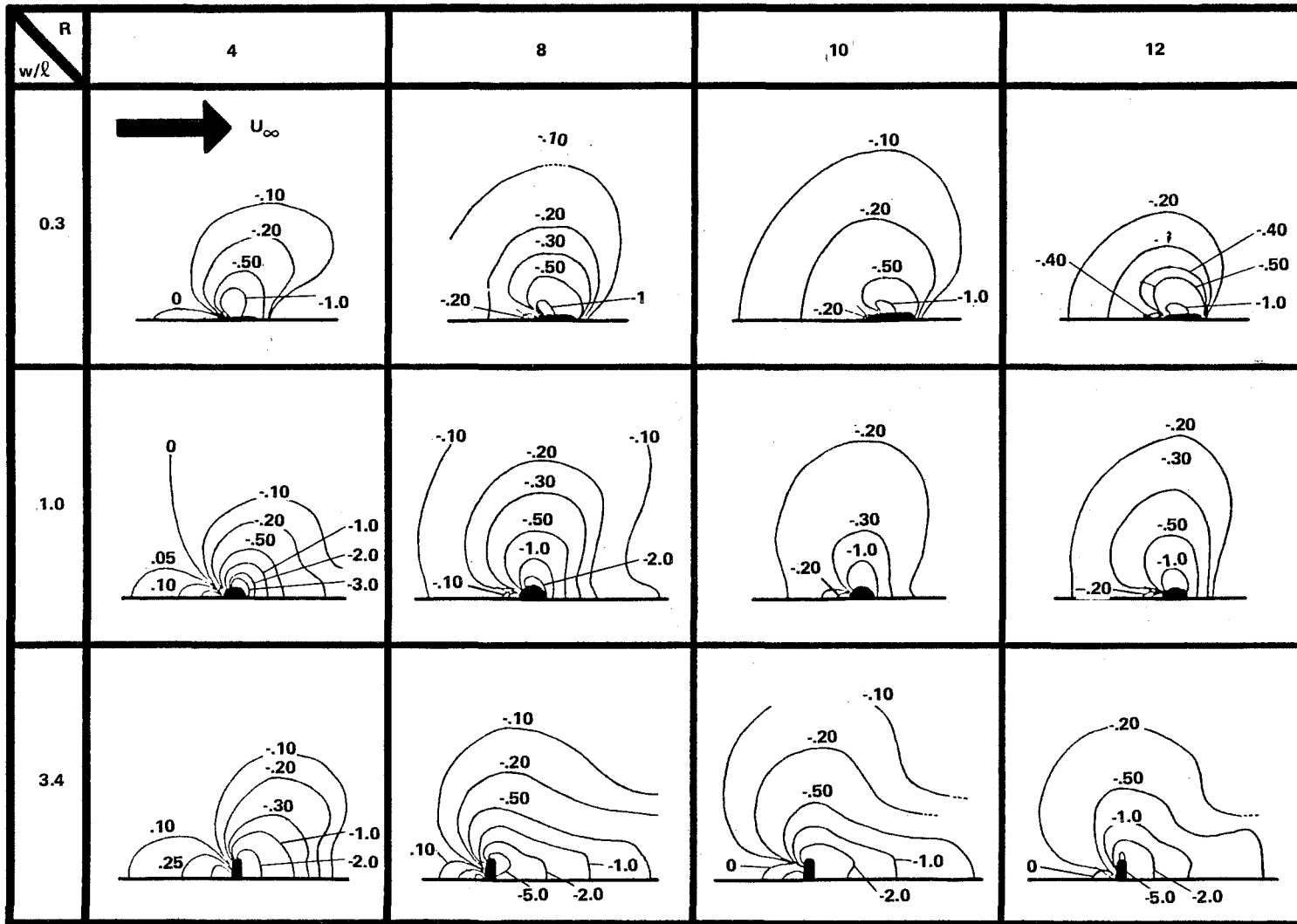


FIGURE 23 - Composite of c_p Contours (reference 19)

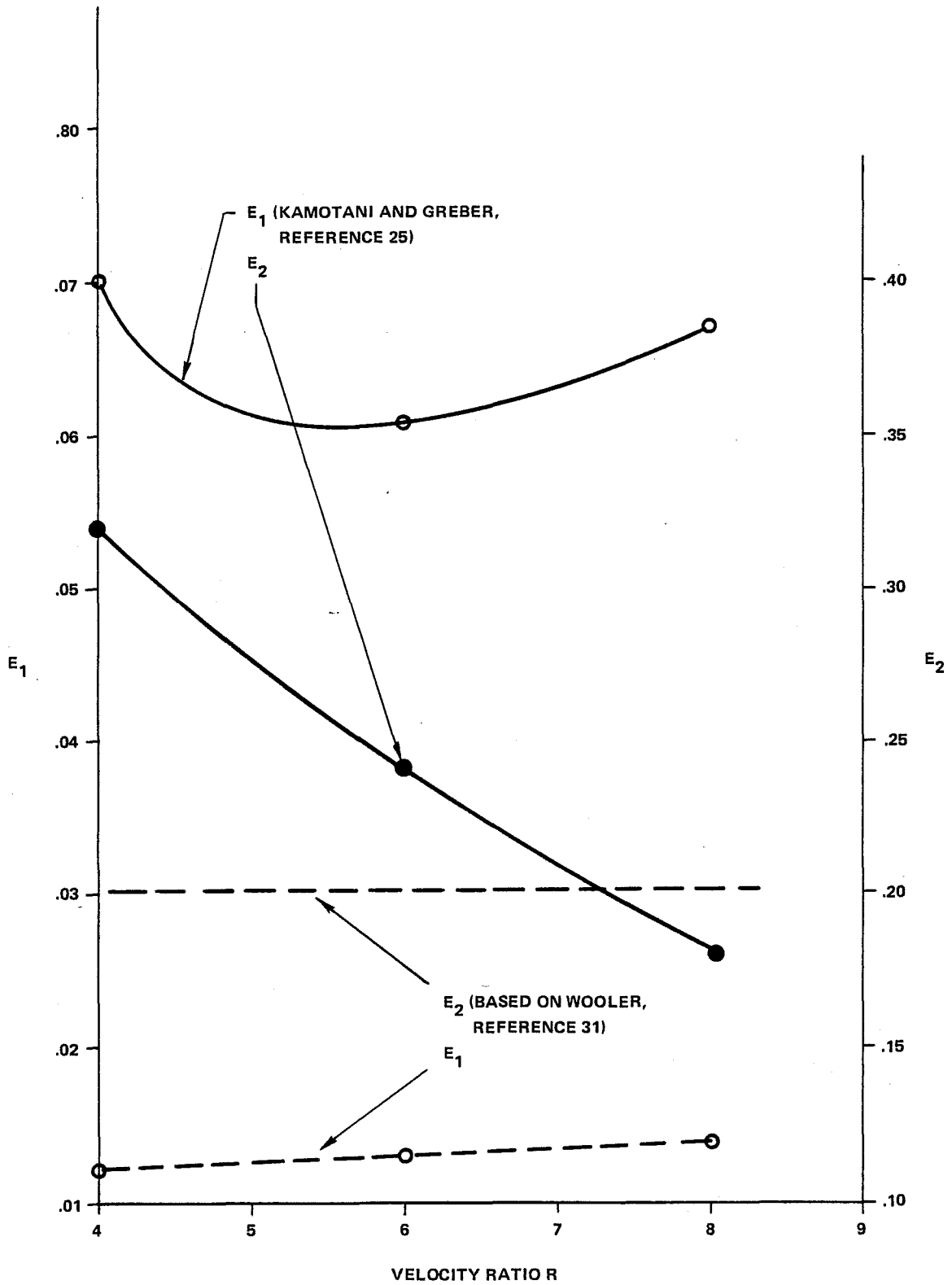


FIGURE 24 - Comparison of Entrainment Coefficients

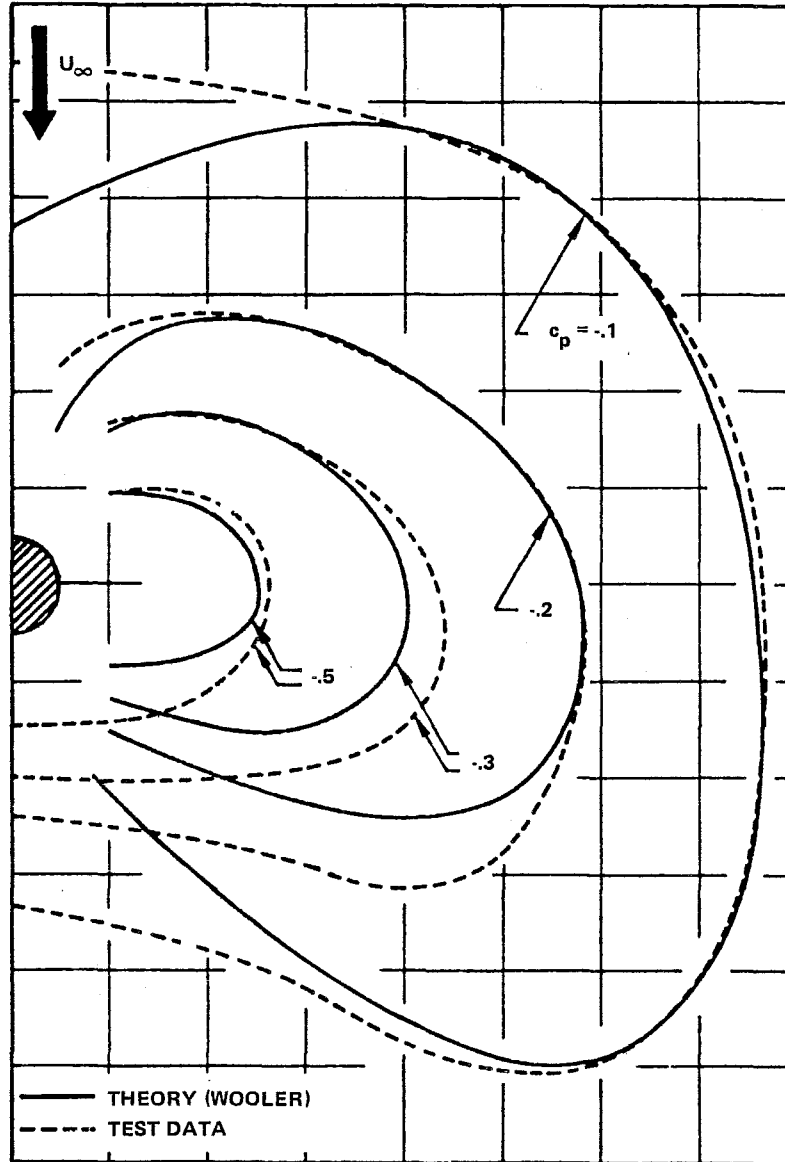


FIGURE 25 - Pressure Distribution Around a Single Jet Issuing at an Angle $\omega = 90^\circ$, $R = 8$

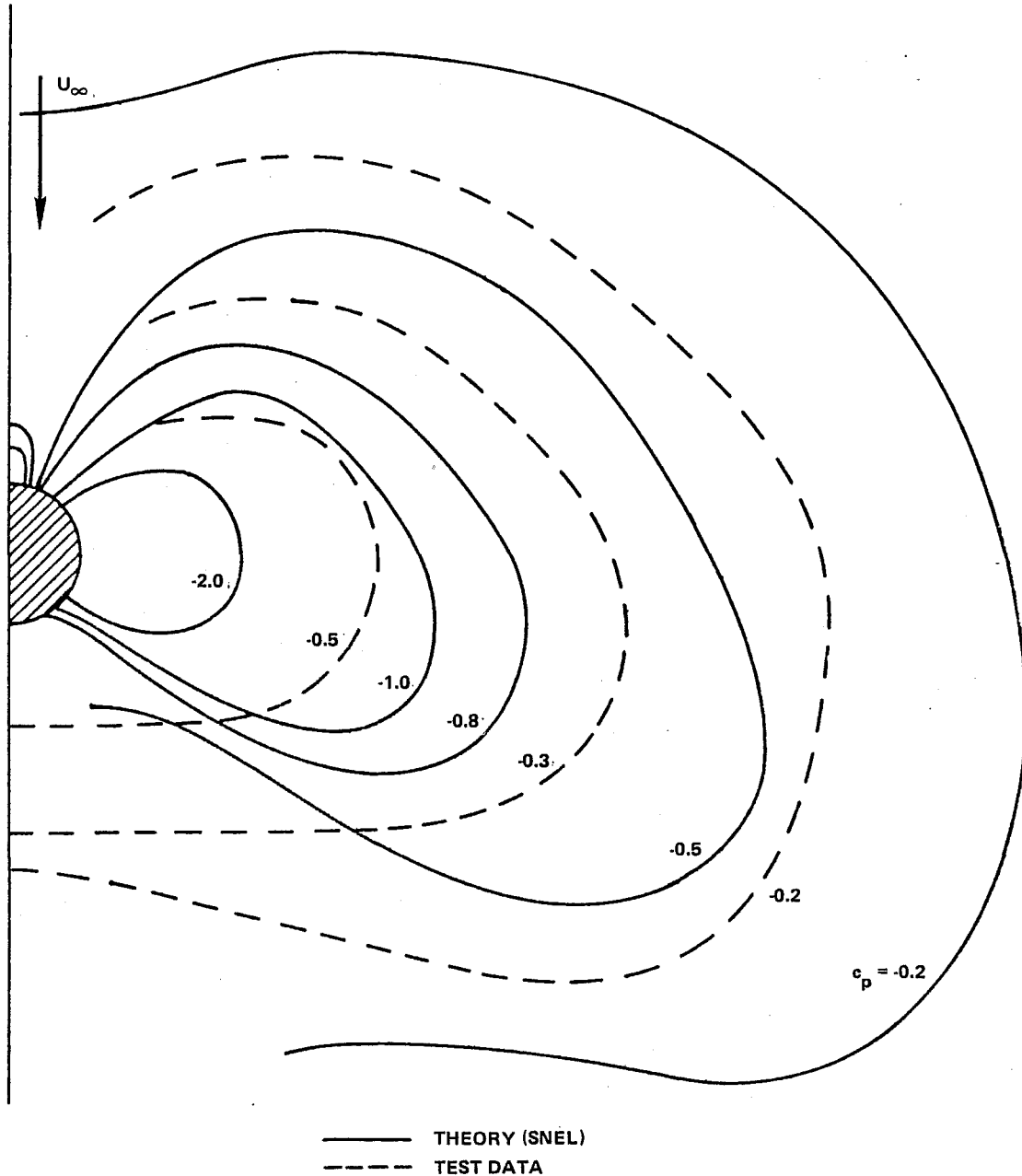


FIGURE 26 - Pressure Distribution Around a Single Jet Issuing at an Angle $\omega = 90^\circ$, $R = 8$

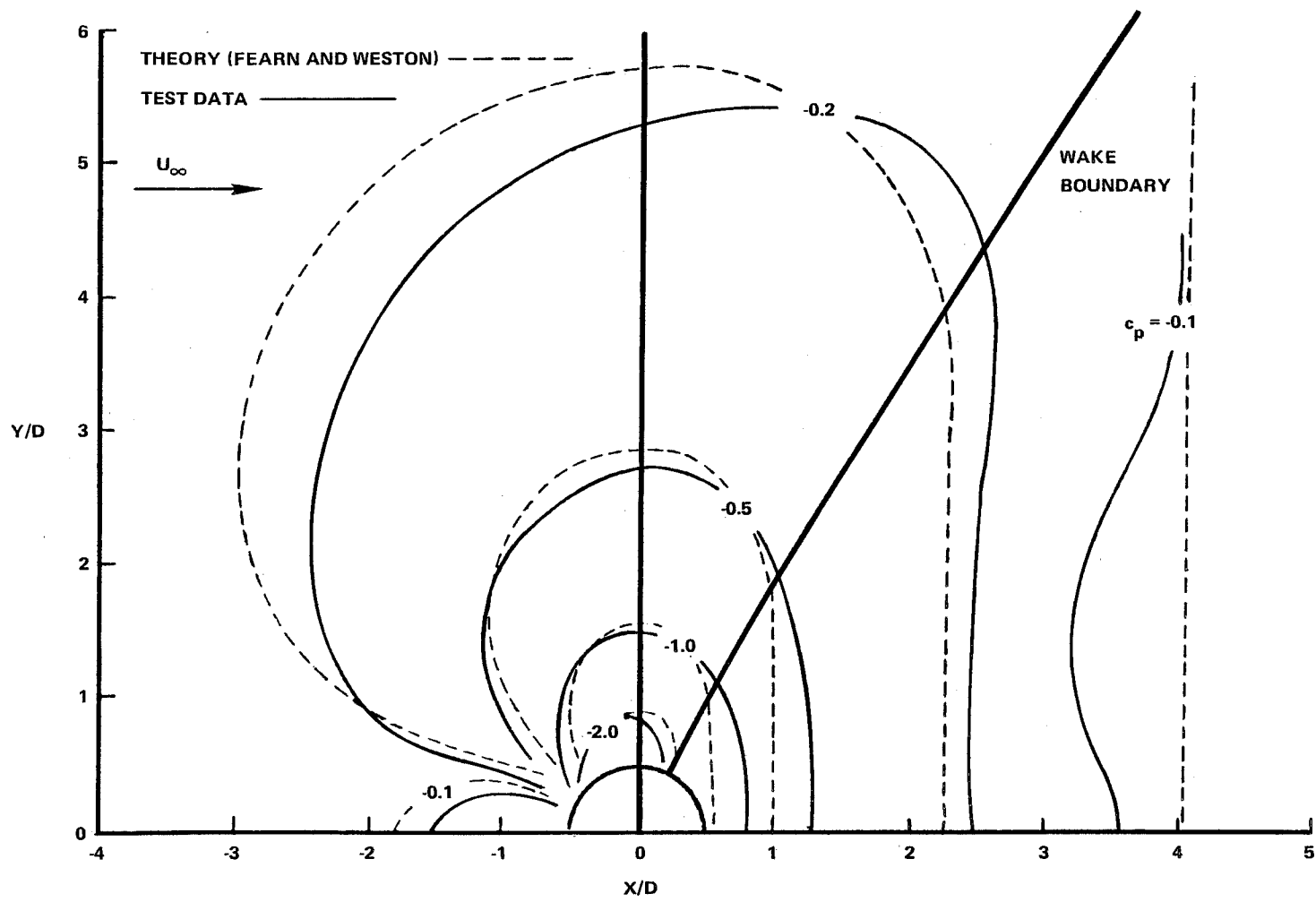


FIGURE 27 - Pressure Distribution Around a Single Jet Issuing at an Angle $\omega = 90^\circ$, $R = 8$

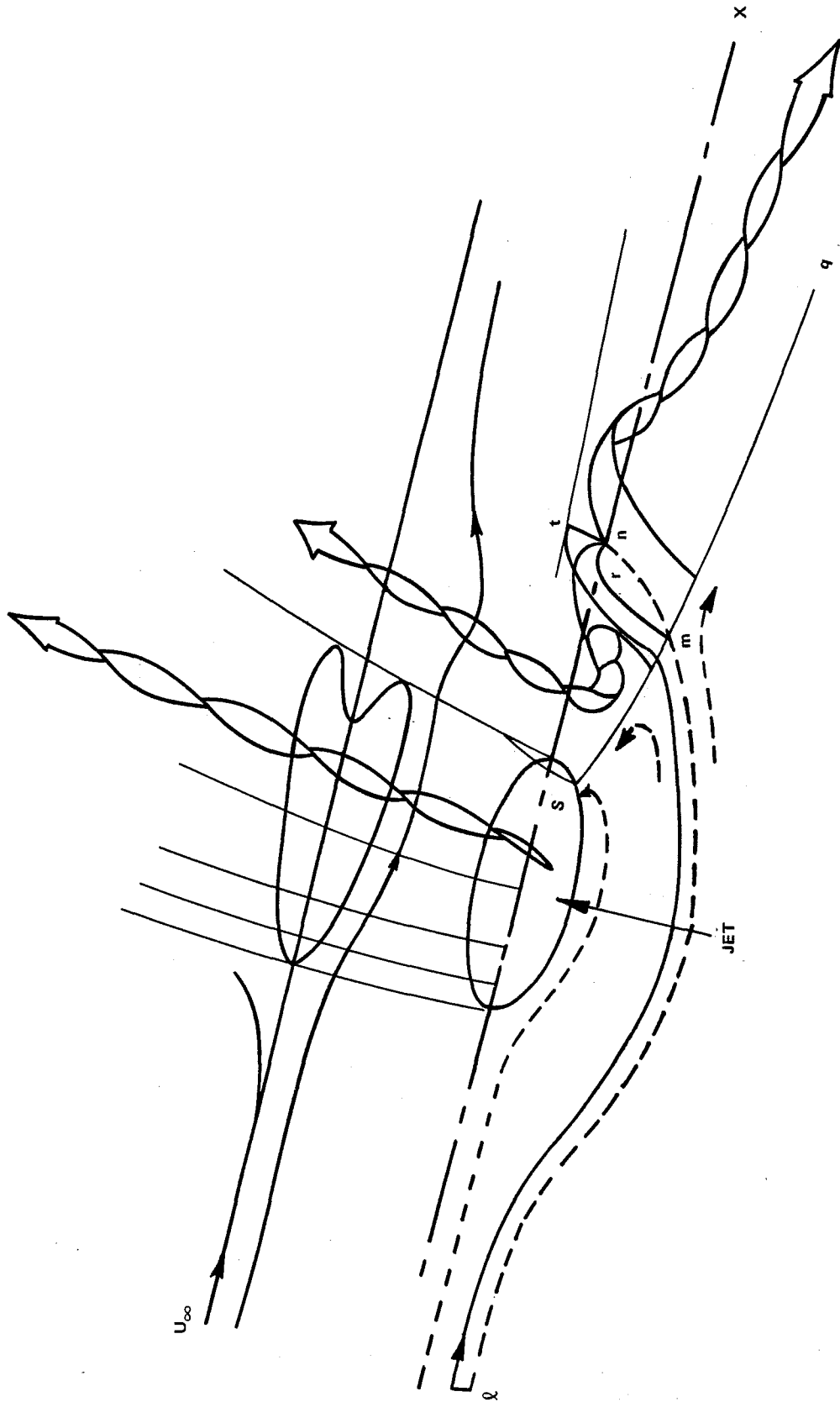


FIGURE 28 - A Sketch of the Flow Pattern

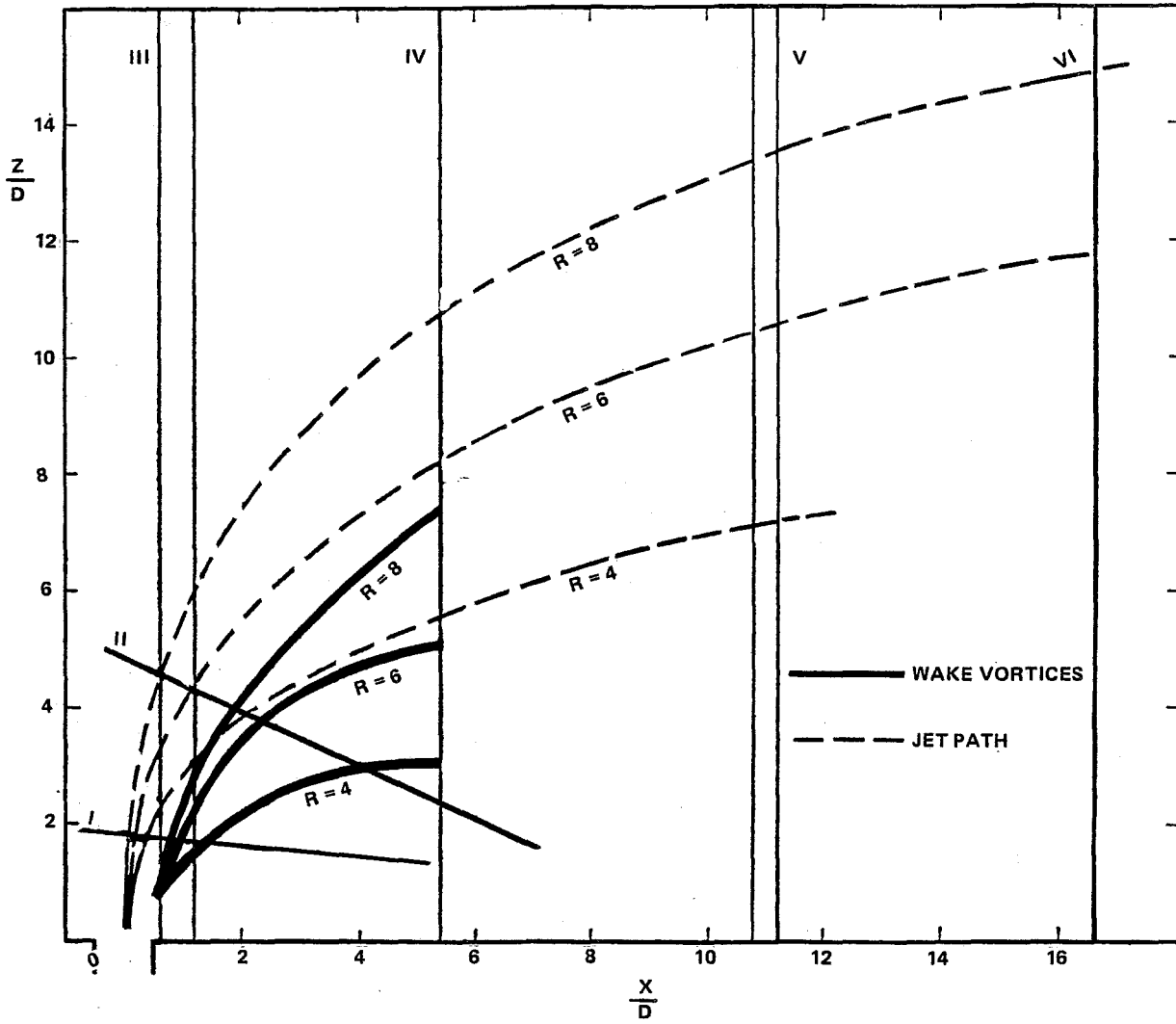


FIGURE 29 - Location of the Wake Vortices

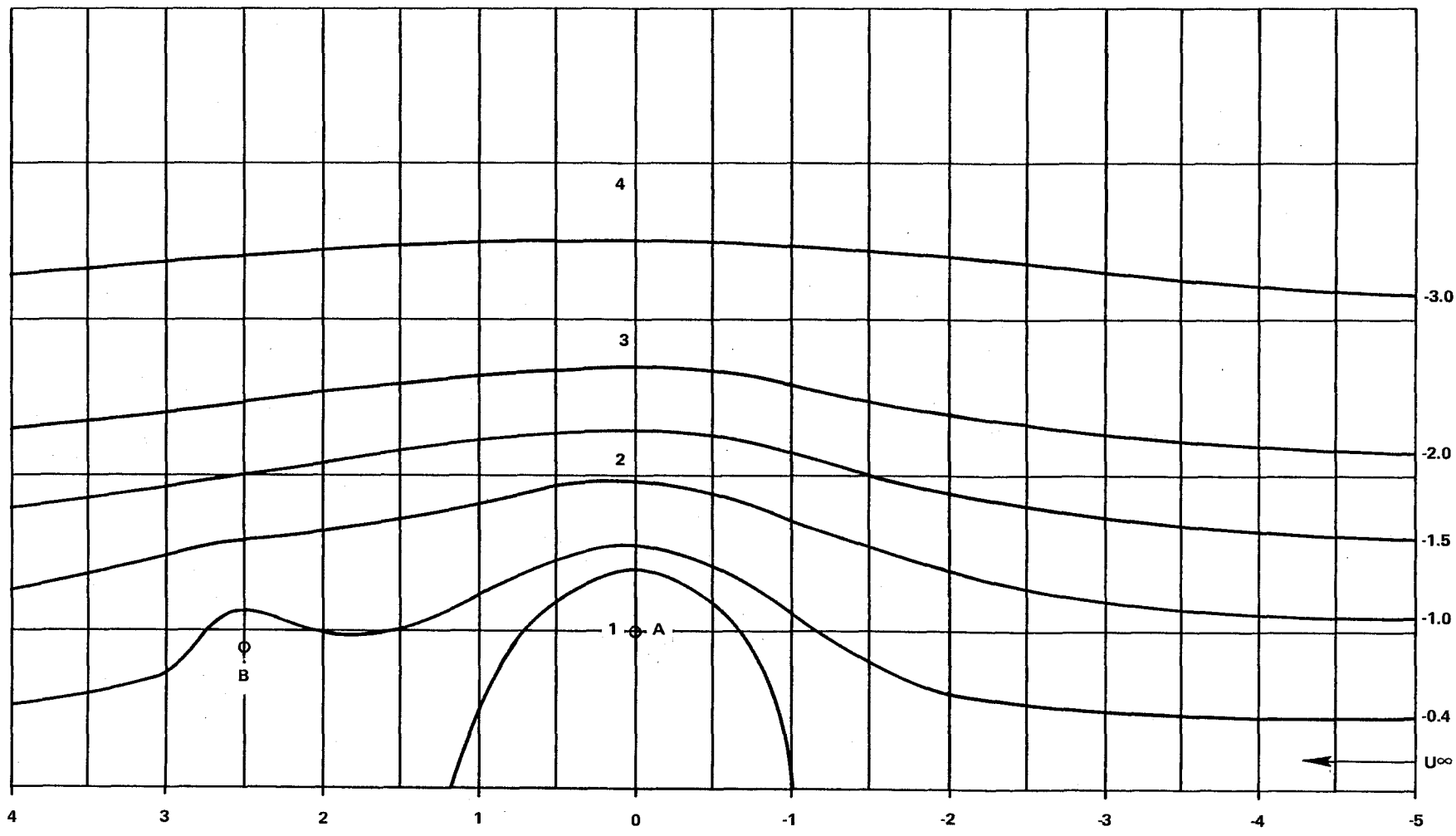


FIGURE 30 - Flow Over a Body - Closed Streamlines

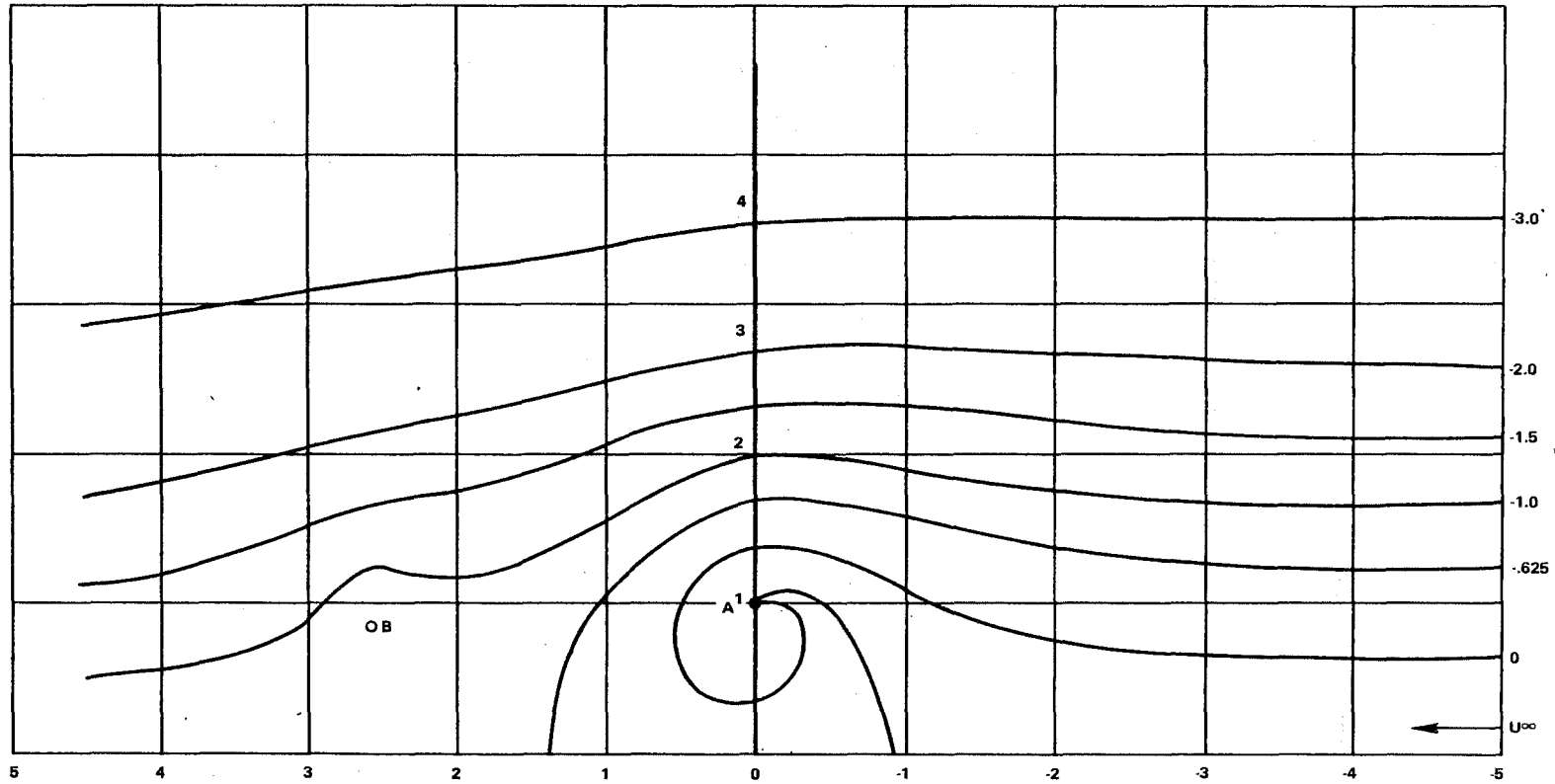


FIGURE 31 - Flow With Open Streamlines

DISTRIBUTION LIST (Continued)

REPORT NO. NADC-78291-60

AIRTASK NO. A3203200/001A/9R023-02-000

	<u>No. of Copies</u>
Computational Mechanics, Knoxville, TN	1
Univ of Florida, Gainesville, FL (Attn: Dr. R. Fearn)	1
Georgia Inst of Technology, Aerospace Engrg, Atlanta, GA (Attn: Dr. H. McMahon)	1
Penn State Univ, Aerospace Engrg, University Park, PA (Attn: Professor B. W. McCormick)	1
DDC	12

D I S T R I B U T I O N L I S T

REPORT NO. NADC-78291-60

AIRTASK NO. A3203200/001A/9R023-02-000

	<u>No. of Copies</u>
CDR, NAVWEPCEN, China Lake	1
CO, NAVAIRPROTESCEN, Trenton, NJ	1
David Taylor NAVSHIP R&D CTR, Bethesda, MD	2
(1 for H. Chaplin)	
(1 for T. C. Tai)	
ONR, Arlington, VA	2
(1 for D. Siegel)	
(1 for M. Cooper)	
Supt, NAVPOSTGRADSCL, Monterey, CA	2
(1 for L. Schmidt)	
(1 for M. Platzter)	
Dir, NASA Ames Research Ctr, Moffet Field, CA	2
(1 for D. Hickey)	
(1 for W. Deckert)	
Dir, NASA Langley Research Ctr, Hampton, VA (Attn: R. Margason)...	1
Dir, NASA, Cleveland, OH	1
Dir, AF FLTDYNLAB (ASD/ENFDH), Wright-Patterson AFB, Dayton, OH ..	1
CDR, AF AERSYSDIV, Wright-Patterson AFB, Dayton, OH	1
CO, USA RES Office, Research Triangle Park, NC	1
CG, Army Aviation Sys Command, St. Louis, MO	1
Boeing Co., Seattle, WA (Attn: E. Omar)	1
LTV Aerospace Corp., Dallas, TX (Attn: T. Beatty, W. Simpkin)...	1
Rockwell International, Columbus, OH (Attn: W. Palmer)	1
General Dynamics Corp., Ft. Worth, TX (Attn: W. Folley)	1
NAVAIRSYSCOM	4
(2 for AIR-950D)	
(1 for AIR-320D)	
(1 for AIR-5301)	
Nielson Engineering, Mountain View, CA (Attn: S.B.Spangler)	1
Duvvuri Research Co., Chula Vista, CA	1
Univ of Tennessee, Space Inst, Tullahoma, TN (W. F. Jacobs)	1
Lockheed-Calif Co., Burbank, CA (Attn: Y. T. Chin)	1
Northrop Corp., Hawthorne, CA	2
(1 for P. T. Wooler)	
(1 for W. H. T. Loh)	
Grumman Aerospace Corp., Bethpage, LI, NY (Attn: D.Migdal)	1
Royal Aeronautical Establishment, Bedford, England.	
(Attn: A. Woodfield)	1
Fairchild-Republic Corp., Farmingdale, LI, NY	1
Calspan, Buffalo, NY	1
McDonnell Douglas Corp., St. Louis, MO	2
(1 for C. Miller)	
(1 for W. Bower)	

(Continued on inside)